Journal of Clinical and Translational Hepatology **2026** vol. 14(8) | 824–841
DOI: 10.14218/JCTH.2026.00106

Original Article

Integrative Multi-omics and Machine Learning Reveal the Therapeutic Mechanisms of Juanyu-Xiaozhi Formula in Metabolic Dysfunction-associated Steatotic Liver Disease and Hepatic Fibrosis via the AP-1/PPARγ/SCD1 Axis

Zhiqiang Jin[1#], Yi Huang[2#], Cheng Zeng[3], Yueting Zhang[2], Yu Qiu[2], Yang Yang[2,1*] and Huabao Liu[2*]

[1]Department of Infectious Diseases, Key Laboratory of Molecular Biology for Infectious Diseases (Ministry of Education), Institute for Viral Hepatitis, the Second Affiliated Hospital, Chongqing Medical University, Chongqing, China; [2]Department of Liver Diseases, the First Affiliated Hospital of Chongqing University of Chinese Medicine, Chongqing, China; [3]Department of Gastroenterology, the First Affiliated Hospital, Chongqing Medical University, Chongqing, China

Received: February 05, 2026 | **Revised:** June 02, 2026 | **Accepted:** July 16, 2026 | **Published online:** August 07, 2026

Abstract

Background and Aims: Despite the surging global prevalence of metabolic dysfunction-associated steatotic liver disease (MASLD) and related liver fibrosis, effective treatments remain limited. While the traditional Chinese medicine Juanyu-Xiaozhi Formula (JYXZF) is used against MASLD, its bioactive components and mechanisms are poorly understood. This study aimed to investigate the therapeutic effects of JYXZF and elucidate its underlying mechanisms of action. ***Methods:*** The constituents of JYXZF were characterized using ultra-high-performance liquid chromatography–tandem mass spectrometry (UPLC-MS/MS). Its efficacy was evaluated in a rat model of metabolic dysfunction-associated steatohepatitis (MASH) induced by a high-fat/calorie diet with high-fructose/high-glucose water, utilizing serum biochemistry, histology, and glucose/insulin tolerance tests. Mechanistic validation was performed in free fatty acid-treated human hepatocellular carcinoma cell line HepG2 (HepG2) cells and HepG2/human hepatic stellate cell line LX-2 (LX-2) co-culture models using luciferase assays, chromatin immunoprecipitation-quantitative polymerase chain reaction (ChIP-qPCR), and activator protein 1 (AP-1) overexpression rescue experiments. The functional relevance of stearoyl-CoA desaturase 1 (SCD1) was further assessed *in vivo* through liver-targeted adeno-associated virus (AAV)-mediated *Scd1* overexpression. ***Results:*** Flavonoids were identified as the main bioactive constituents. JYXZF administration alleviated metabolic dysfunction, reduced hepatic lipid accumulation, and attenuated inflammation and fibrosis in MASH rats. Multi-omics integration and machine learning-assisted target prioritization identified lipid metabolic and inflammatory pathways. Among these pathways, we selected the AP-1/peroxisome proliferator-activated receptor gamma (PPARγ)/SCD1-related lipogenic pathway for functional validation. Target perturbation experiments supported the functional involvement of AP-1 in the regulation of the PPARγ/SCD1 pathway and its contribution to the anti-steatotic effects of JYXZF. ***Conclusions:*** JYXZF alleviates MASLD-associated steatosis and fibrosis via the AP-1/PPARγ/SCD1-related lipogenic axis, demonstrating its therapeutic potential for MASLD/MASH and providing a mechanistic basis for future clinical applications.

Citation of this article: Jin Z, Huang Y, Zeng C, Zhang Y, Qiu Y, Yang Y, *et al*. Integrative Multi-omics and Machine Learning Reveal the Therapeutic Mechanisms of Juanyu-Xiaozhi Formula in Metabolic Dysfunction-associated Steatotic Liver Disease and Hepatic Fibrosis via the AP-1/PPARγ/SCD1 Axis. J Clin Transl Hepatol 2026;14(8):824–841. doi: 10.14218/JCTH.2026.00106.

Introduction

Metabolic dysfunction-associated steatotic liver disease (MASLD) is a widespread chronic metabolic condition. Its global incidence has risen steadily with the increasing prevalence of obesity and type 2 diabetes, currently affecting nearly 38% of the global population.[1,2] Recent studies indicate that MASLD is characterized by chronic metabolic dysfunction, which leads to abnormal lipid deposition in the liver. Prolonged fat accumulation causes fatty degeneration and sensitizes the liver to oxidative stress, lipotoxicity, and chronic inflammation, which ultimately drive hepatocellular injury and fibrosis. Consequently, these changes substantially increase the risk of adverse clinical outcomes.[3,4] Although substantial progress has been made in the diagnosis and treatment of MASLD, pharmacological treatment options remain limited. The development of new drugs or combination therapies that provide long-term control of metabolic disorders is essential

Keywords: Flavonoids; Juanyu-Xiaozhi Formula; Lipid metabolism; Traditional Chinese Medicine; MASH; Machine Learning; Metabolomics; Multi-omics; PPAR; SCD1.

[#]Contributed equally to this work.

[*]**Correspondence to:** Huabao Liu and Yang Yang, Department of Liver Diseases, the First Affiliated Hospital of Chongqing University of Chinese Medicine, Chongqing 400013, China. ORCID: https://orcid.org/0009-0006-9340-1728 (YY). Tel/Fax: +86-23-67063760, E-mail: 15909386658@163.com (HL) and yangyangxd95@163.com (YY).

to improve patient care.[5] Therefore, the identification of new therapeutic agents is important for expanding treatment options for MASLD.

Previous studies have shown that the liver is the central regulator of lipid metabolism.[6] Excessive dietary lipid intake increases the metabolic burden on the liver and promotes hepatic steatosis to varying degrees. This process contributes to disease progression across the MASLD spectrum, from relatively benign simple steatosis to progressive fatty liver inflammation (metabolic dysfunction-associated steatohepatitis [MASH]), fibrosis, and cirrhosis.[7] Excessive lipid accumulation in the liver forms the pathological basis of MASLD. The disease is associated with cardiovascular and metabolic risk factors, including overweight or obesity (especially abdominal obesity), hypertension, dyslipidemia, and type 2 diabetes. Research indicates that insulin resistance and type 2 diabetes are key drivers of MASLD because they increase the mobilization of free fatty acids (FFAs) from adipose tissue, promote hepatic triglyceride production, and lead to persistent hepatic fat accumulation.[8,9] These changes trigger inflammatory responses and metabolic dysfunction, disrupt liver metabolic zonation, and promote metabolic reprogramming.

The peroxisome proliferator-activated receptor (PPAR) family represents a key therapeutic target for MASLD. For example, lanifibranor, which has received Breakthrough Therapy designation from the U.S. Food and Drug Administration (FDA), is a broad-spectrum PPAR agonist that improves insulin sensitivity and lipid metabolism and can reverse MASH and liver fibrosis.[10] Among the PPAR subtypes, PPARγ plays an important role in lipid metabolism. Numerous studies have shown that PPARγ promotes lipid accumulation by binding to PPAR response elements and activating genes involved in de novo lipogenesis,[11] including fatty acid translocase and stearoyl-CoA desaturase 1 (SCD1). PPARγ also regulates inflammatory responses and insulin sensitivity,[12–14] making it an attractive target for metabolic syndrome and related diseases.

In recent years, traditional Chinese medicine (TCM) has attracted increasing attention because of its therapeutic effects and relatively few adverse effects. Existing research indicates that TCM shows promise in the treatment of MASLD, as demonstrated by the Shenge Formula.[15] Therefore, TCM-based strategies that regulate hepatic lipid metabolism represent a scientifically sound and feasible approach to controlling hepatic steatosis. The Juanyu-Xiaozhi Formula (JYXZF) is derived from the TCM prescriptions recorded in *Jin Gui Yao Lue* and was summarized by Professor Huabao Liu, a nationally renowned TCM practitioner, based on the TCM theory that "the liver governs the regulation of qi dynamics"[16] and his extensive clinical experience. Extensive clinical observations show that JYXZF effectively reduces hepatic steatosis and fibrosis.[17] It consists of five herbs: *Monascus purpureus* Went (Hong qu), *Gynostemma pentaphyllum* (Thunb.) Makino (Jiao gulan), *Artemisia scoparia* Waldst. & Kit. (Yin chen), *Cassia obtusifolia* L. (Jue Mingzi), and *Curcuma longa* L. (Jiang huang), which is commonly used to treat fatty liver disease. Modern pharmacological studies have shown that these five herbs produce significant lipid-lowering effects.[18–22] However, the specific mechanisms of action and key therapeutic targets of JYXZF remain unclear.

This study explored the therapeutic effects of JYXZF on MASLD/MASH and investigated the potential molecular networks associated with its activity. We identified the bioactive components of JYXZF using ultra-high-performance liquid chromatography-mass spectrometry (UPLC-MS). We also used a JYXZF-treated MASH rat model and combined transcriptomics and metabolomics with a multimodal prediction approach based on multiple databases. Machine learning-assisted analyses were used to prioritize candidate targets for subsequent experimental validation. These findings offer novel insights into the therapeutic mechanisms of JYXZF in the treatment of MASLD/MASH.

Methods

Preparation of JYXZF extract

JYXZF is composed of a combination of multiple traditional Chinese herbs: *Monascus purpureus* Went (used for fermenting rice, 12 g/batch), *Gynostemma pentaphyllum* (whole herb, 30 g/batch), *Artemisia scoparia* Waldst. & Kit. (aboveground parts, 15 g/batch), *Cassia obtusifolia* L. (seeds, 12 g/batch), and *Curcuma longa* L. (rhizome, 10 g/batch). Raw herbs were purchased from Beijing Kangrentang Pharmaceutical Company (China) and authenticated according to the Chinese Pharmacopoeia. The formula was prepared at Chongqing Traditional Chinese Medicine Hospital following the patented composition (patent number: ZL 202411543696.2).

For extract preparation, 100 batches of crude herbs (equivalent to 7,900 g) were decocted in 20 L of purified water at 100 °C. The supernatant was then concentrated to 363.9 mL and stored at 4 °C.[15] The final concentration was 21.71 g/mL. The rat-equivalent dose was calculated from the clinically used human dose by body surface area conversion and corresponded to 5.428 g/kg/day.

Animals and treatment

All SPF-grade male Sprague-Dawley (SD) rats (6 weeks old) were housed at the Chongqing Medical University Laboratory Animal Centre. Animals were maintained under SPF conditions at 20–24 °C, 40–70% humidity, and a 12-h light/dark cycle, with free access to food and water. Animal feeding, care, sample collection, and all experimental procedures complied with the regulations of the Ethics Committee of Chongqing Medical University (license number: IACUC-SAH-CQMU-2025-0141) and Chongqing Traditional Chinese Medicine Hospital (license number: 2024-DWSY-YY).

After a 2-week acclimation period, 8-week-old rats were randomly assigned to six groups (n = 6 per group): normal control (Con), high-fat/calorie diet with high-fructose/high-glucose water (MASH),[23] low-, medium-, and high-dose JYXZF treatment groups (JYXZF-L, JYXZF-M, JYXZF-H), and obeticholic acid (OCA) treatment. The control group received a standard maintenance diet. All other groups received the MASH diet for 20 weeks. The diet consisted of a high-fat/high-calorie diet (60% kcal from fat; D12492, Research Diets, New Brunswick, NJ, USA) and drinking water supplemented with 23.1 g/L D-fructose and 18.9 g/L D-glucose. The JYXZF groups received low-, medium-, and high-dose JYXZF by oral gavage. JYXZF was prepared at a fixed concentration of 21.71 g/mL and administered at 25, 50, or 100 μL/day, respectively. The high dose (100 μL/day) corresponded to the clinically effective human dose after body surface area normalization. Rats in the OCA group received OCA (10 mg/kg, MedChemExpress, HY-12222) by oral gavage. Body weights were recorded weekly. After 12 weeks of treatment, rats were sacrificed, and tissues were collected for subsequent experiments.

Glucose/insulin tolerance tests (GTTs/ITTs) and biochemical analysis

GTTs were performed after 16 h of fasting by intraperitoneal injection of glucose (1 g/kg). ITTs were performed after 6 h of fasting by intraperitoneal injection of insulin (0.5 IU/

kg). Blood glucose was measured at 0, 15, 30, 60, and 120 min. The area under the curve (AUC; 0–120 min) was calculated using the trapezoidal rule.[24] Serum levels of alanine aminotransferase (ALT), aspartate aminotransferase (AST), triglycerides (TG), total cholesterol (TC), high-density lipoprotein cholesterol (HDL-C), and low-density lipoprotein cholesterol (LDL-C) were measured using an automated biochemical analyzer. Liver levels of tumor necrosis factor alpha (TNF-α) and interleukin-6 (IL-6) levels were measured using enzyme-linked immunosorbent assay kits.[25]

Histology

Liver tissues were fixed in 4% paraformaldehyde, embedded in paraffin, and stained with H&E and Sirius Red. Frozen liver sections were stained with Oil Red O to visualize lipid accumulation.[25] Representative images were acquired using a digital slide scanner. Histological assessment was performed under blinded conditions. Images were coded before analysis, and investigators responsible for evaluation were unaware of group allocation.

Ultra-high-performance liquid chromatography–tandem mass spectrometry (UPLC-MS/MS) analysis of JYXZF prototypes and circulating metabolites

JYXZF decoction, blank serum, JYXZF mixed with blank serum, and serum from JYXZF-treated rats were analyzed by UPLC-MS/MS using a Vanquish UHPLC system coupled to a Q-Exactive HFX mass spectrometer. Raw data were converted to mzXML format using ProteoWizard and processed using XCMS for peak alignment, retention time correction, and peak extraction according to previously published workflows.[26,27] Compounds were annotated by matching accurate mass, isotope pattern, retention time, adduct type, and MS/MS fragmentation patterns against an in-house TCM high-resolution mass spectral database and public libraries, including GNPS, ReSpect, MassBank, HMDB, and METLIN.[28–30] The main identification criteria were a precursor mass error <25 ppm and an MS/MS spectral matching score >0.7. High-response annotations were manually verified based on peak shape and fragmentation consistency. Blank serum features were excluded unless they showed a substantial increase after JYXZF administration. Compounds detected in both the decoction and treated serum were annotated as absorbed prototypes. Serum features that showed plausible biotransformation patterns were annotated as circulating metabolites.

Untargeted metabolomics

Untargeted metabolomics was performed by UPLC-Q Exactive high-resolution mass spectrometry in positive and negative ion modes.[26,31] Quality control (QC) samples were prepared by pooling equal aliquots from all study samples. QC samples were injected at regular intervals to monitor analytical stability and signal drift. Raw data were processed using Progenesis QI v3.0 for peak detection, alignment, deconvolution, QC-based normalization, and metabolite annotation. Features with poor QC reproducibility were excluded. Metabolites were annotated against HMDB, LipidMaps, METLIN, and LuMet-Animal 3.0 using retention time, accurate mass, isotope distribution, and MS/MS fragmentation patterns. Principal component analysis (PCA), orthogonal partial least squares discriminant analysis (OPLS-DA), and 200 permutation tests were performed. Differential metabolites were defined as $P < 0.05$ and a fold change ≥1.5 or ≤0.67.

Hepatic transcriptomics and enrichment analyses

Total RNA was extracted from liver tissues using TRIzol reagent. RNA-seq libraries were constructed using the VAHTS Universal V6 RNA-seq Library Prep Kit and sequenced by OE Biotech Co., Ltd. Gene count matrices were analyzed using R software. Differential expression analysis was performed with DESeq2.[32] Genes with a q-value < 0.05 and an absolute $\log_2$ fold change > 1 were defined as differentially expressed genes (DEGs). Gene Ontology (GO), Kyoto Encyclopedia of Genes and Genomes (KEGG), Reactome, and WikiPathways enrichment analyses were performed using a hypergeometric test.[33]

Multi-omics integration, weighted gene co-expression network analysis (WGCNA), network pharmacology, and machine learning

DEGs and differential metabolites were integrated to identify concordant transcriptional and metabolic programs associated with JYXZF treatment. WGCNA was performed in R after $\log_2$ transformation of gene expression data and Z-score normalization of metabolite abundance.[34] Modules were identified using dynamic tree cutting. Module-metabolite associations were evaluated by gene significance and module membership.

MASLD-related genes were retrieved from OMIM, GeneCards, DisGeNET, and TTD.[35–37] JYXZF-related compounds and targets were obtained from TCMSP, HERB, SwissADME, SwissTargetPrediction, and UniProt.[38–41] Protein–protein interaction (PPI) networks were constructed using STRING and visualized in Cytoscape.[42,43] Machine learning was used for candidate target prioritization rather than causal inference.[44] Candidate targets identified by network pharmacology and multi-omics integration served as input features, and experimental group labels were used as outcome variables. Least absolute shrinkage and selection operator (LASSO) regression, support vector machine (SVM) modeling, and neural network modeling were constructed using the glmnet, e1071, and nnet packages in R, respectively. Public Gene Expression Omnibus (GEO) datasets from MASLD models were used for disease-context validation.

Molecular docking and molecular dynamics simulation

Representative circulating constituents were selected as ligands based on UPLC-MS/MS annotation confidence and structural categories. Ligand structures were obtained from PubChem. Protein structures of PPARγ and the activator protein 1 (AP-1) Jun proto-oncogene (JUN)/Fos proto-oncogene (FOS) dimer were retrieved from the RCSB Protein Data Bank.[45] Molecular docking was performed using CB-Dock2.[46] Molecular dynamics simulations were performed using GROMACS[47,48] to evaluate complex stability. Root-mean-square deviation (RMSD), radius of gyration (Rg), root-mean-square fluctuation (RMSF), and ligand–protein distance were calculated.

Cell culture and processing

Human hepatocellular carcinoma cell line HepG2 (HepG2) cells were stored in our laboratory. Cells were cultured in Dulbecco's Modified Eagle Medium (DMEM, SH30243.01, HyClone, Logan, UT, USA) supplemented with 10% fetal bovine serum (FBS, Gibco, Rockville, MD, USA) and penicillin-streptomycin solution (04481229, Adamas Life). Cells in the treatment group were first cultured in 0.5 mM FFAs (palmitic acid:oleic acid = 2:1) for 24 h to induce steatosis. Cells were then treated with JYXZF-medicated serum, individual purified compounds, the four-compound mixture, or OCA (HY-12222, MedChemExpress).

For co-culture experiments, human hepatic stellate cell line LX-2 (LX-2) cells were seeded into 12-well plates. FFA-induced HepG2 cells were seeded onto polyester Transwell inserts (BIOFIL, Guangzhou, China) and allowed to adhere overnight. The inserts were then placed into the LX-2 wells and co-cultured for 48 h in DMEM containing 2% FBS. After co-culture, the Transwell inserts were removed, and both cell types were collected immediately for subsequent analysis.[49]

Cell Counting Kit-8 (CCK-8) assay

Cell viability was assessed with the CCK-8 (C0005, TargetMol, Boston, MA, USA). Approximately 1×10^3 cells were seeded into each well of a 96-well plate. Cells were treated with 100 μL of medium containing different concentrations of drug-containing serum and incubated for 72 h. Following treatment, 100 μL of medium containing 10% CCK-8 reagent was added to each well, and the plates were incubated for 30 min at 37 °C. Absorbance (OD) at 450 nm was measured using a microplate reader.

AP-1 knockdown assay

AP-1 loss-of-function experiments were performed in FFA-induced HepG2 cells by siRNA-mediated knockdown of JUN and FOS. Commercially synthesized siRNAs targeting JUN and FOS, the two major components of the AP-1 transcriptional complex, were used. HepG2 cells were co-transfected with si-JUN and si-FOS to suppress AP-1 activity. A non-targeting siRNA served as the negative control. Knockdown efficiency of siRNAs was confirmed by western blot.

Gene overexpression in cells and in vivo adeno-associated virus (AAV) delivery

For the cell experiments, AdFOS, AdJUN, and AdSCD1 adenoviruses were generated using the AdEasy system by Beijing Tsingke Biotech Co., Ltd. (China). Transfection efficiency was confirmed by western blot. For the animal experiments, liver-specific AAV-control and AAV-*Scd1* vectors were purchased from Shanghai Genechem Co., Ltd. (Shanghai, China). Rats received tail vein injections at 10 weeks of age (2×10^{11} genome copies/rat). SCD1 overexpression in rat hepatocytes was confirmed by western blot.

RNA extraction and reverse transcription quantitative polymerase chain reaction (RT-qPCR)

Total RNA was extracted from liver tissue and cultured cells using a total RNA extraction kit. RNA concentration was measured, and RNA was reverse-transcribed into cDNA using a reverse transcription kit. Target gene expression was determined by RT-qPCR. Relative mRNA expression was normalized to Actb and calculated using the $2^{-\Delta\Delta CT}$ method.[50] Primer sequences are provided in the Supplementary File 1.

Western blot

Proteins were extracted from homogenized rat liver tissues using lysis buffer (P0013, Beyotime Biotechnology, Shanghai, China) supplemented with 1% phenylmethylsulfonyl fluoride (PMSF) and 1% phosphatase inhibitor (EpiZyme, Shanghai, China). HepG2 cells were cultured to approximately 60% confluence. Cells were treated with FFA for 24 h and then exposed to different concentrations of drug-containing serum for another 24 h. Proteins were extracted using the same method. Protein concentration was determined using the bicinchoninic acid assay. Proteins were separated by SDS-PAGE and transferred to PVDF membranes (Millipore, Boston, Massachusetts, USA). Membranes were blocked with 5% non-fat milk and incubated overnight with the following antibodies: anti-PPARγ (66936-1-Ig, Proteintech), anti-FOS (66590-1-Ig, Proteintech), anti-JUN (24909-1-AP, Proteintech), anti-β-actin (20536-1-AP, Proteintech), and anti-GAPDH (GB15002-100, Servicebio). After washing with TBST, membranes were incubated with secondary antibodies.[51] Protein signals were detected using a Bio-Rad imaging system (USA). Western blot membranes were retained for record keeping.

Luciferase reporter assay

To test AP-1-dependent regulation of the PPARγ promoter, reporter constructs containing the PPARγ promoter region (including AP-1 binding sites) were cloned upstream of firefly luciferase. Renilla luciferase was used for normalization. Cells were transfected with reporter plasmids, and luciferase activity was measured 48 h post-transfection using a dual-luciferase assay system.[52]

Chromatin immunoprecipitation-quantitative polymerase chain reaction (ChIP-qPCR) assay

ChIP-qPCR was performed to assess c-Jun/c-Fos binding to the predicted AP-1 binding region within the PPARγ promoter. HepG2 cells were cross-linked, lysed, and sonicated to obtain fragmented chromatin. Immunoprecipitation was performed using antibodies against c-Jun and c-Fos. IgG was used as a negative control. Purified DNA was analyzed by qPCR using primers targeting the AP-1 binding region. Enrichment was normalized to input DNA. Primer sequences and antibody details are provided in the Supplementary File 1.[52]

Statistical analysis

All statistical analyses were performed using R software (version 4.4.1) and GraphPad Prism 10.1.2. Data are presented as mean ± standard deviation from at least three independent experiments. Student's t-test or paired t-test was used for comparisons between two groups. One-way ANOVA followed by Tukey's post hoc test was used for multi-group comparisons. Pearson's correlation coefficient (R) was used to assess linear relationships. A P-value < 0.05 was considered statistically significant.

Results

Characterization of JYXZF prototypes and main blood-entry components

To identify the bioavailable constituents of JYXZF, we performed UPLC-MS/MS analysis of JYXZF-treated rat serum (JYXZF-treated group), JYXZF decoction (JYXZF), blank serum (Con), and a mixture of JYXZF decoction with blank serum (JYXZF + Con) (Supplementary Fig. 1A). Comparison of base peak chromatograms in both positive and negative ion modes revealed a complex phytochemical profile in the JYXZF decoction and the serum of JYXZF-treated rats (Supplementary Fig. 1B). In total, we annotated 2,831 prototype compounds and 591 serum compounds from the UPLC-MS/MS data.

NPClassifier-based structural classification[53] showed that the circulating compounds were primarily enriched in the shikimate and phenylpropanoid pathways. Flavonoids were the most abundant class, followed by phenolic acids and phenylpropanoids (Supplementary Fig. 1C). These data indicate that JYXZF delivers a broad range of small molecules into the circulation, with flavonoids and phenylpropanoid derivatives representing the major circulating constituents.

JYXZF administration alleviates hepatic steatosis, inflammation, and fibrosis

To evaluate the effectiveness of JYXZF *in vivo*, we established a MASH SD rat model by feeding the animals an high-fat/calorie diet with high-fructose/high-glucose water (HFCD-HF/G) diet. The rats then received low-, medium-, or high-dose JYXZF by intragastric administration for 12 weeks, whereas OCA served as a positive control (Fig. 1A). Food intake did not differ significantly among the groups, indicating that neither JYXZF nor OCA affected appetite or energy intake (Fig. 1B). The MASH diet substantially increased body weight, liver weight, and the liver-to-body weight ratio. JYXZF and OCA significantly attenuated these changes, and JYXZF produced a clear dose-dependent effect (Fig. 1C).

Serum biochemical analysis showed that JYXZF significantly reduced ALT, AST, TG, TC, LDL-C, and fasting blood glucose levels, while increasing HDL-C levels compared with those in untreated MASH rats (Fig. 1D and E). ITTs, GTTs, and the corresponding AUC (0–120 min) analyses demonstrated that JYXZF substantially improved systemic insulin sensitivity in MASH rats and produced greater improvements than OCA (Supplementary Fig. 2A and B). JYXZF also reduced hepatic TNF-α and IL-6 levels, further supporting its anti-inflammatory effects (Supplementary Fig. 2C). Histopathological evaluation revealed extensive macrovesicular steatosis and accumulation of hepatic lipid droplets in MASH rats. JYXZF treatment, especially in the high-dose group, substantially improved these histological abnormalities. H&E staining showed reduced steatosis, Oil Red O staining revealed fewer lipid droplets, and collagen deposition was reduced (Fig. 1F). Together, these findings indicate that JYXZF effectively ameliorated hepatic steatosis, inflammation, and fibrosis in the MASH rat model.

To further confirm the lipid-lowering effects of JYXZF *in vitro*, we established an FFA-induced steatosis model in HepG2 cells and treated the cells with JYXZF-medicated serum. JYXZF-medicated serum reduced lipid accumulation compared with control serum without compromising cell viability. It also significantly lowered intracellular TG and TC levels in HepG2 cells (Supplementary Fig. 2D–F). Because extracellular matrix deposition by hepatic stellate cells (HSCs) is considered a key event in liver fibrosis, we established an FFA-induced HepG2/LX-2 co-culture model to examine HSC activation after JYXZF treatment (Supplementary Fig. 2G). RT-qPCR showed that the mRNA levels of fibrosis markers ACTA2 (α-SMA), COL1A1, COL3A1, TIMP-1, and inflammatory cytokines (TNF-α and IL-6) increased in co-cultured LX-2 cells. JYXZF and OCA significantly reduced the expression of these genes (Supplementary Fig. 2H). Combined with the *in vivo* data, these results demonstrate that JYXZF consistently suppresses hepatic steatosis and attenuates inflammatory and fibrotic changes in both animal and cellular models.

Metabolomics analysis reveals PPAR-related lipid metabolism regulated by JYXZF

To investigate the metabolic effects of JYXZF treatment, we performed untargeted serum metabolomic analysis in MASH rats with or without JYXZF. PCA and OPLS-DA showed clear separation between the MASH group and JYXZF-treated groups. This observation indicated that JYXZF substantially altered the metabolic profile (Supplementary Fig. 3A and B). The OPLS-DA loading plot and S-plot identified the key metabolites that contributed to group separation, and permutation testing confirmed the robustness of the model (Supplementary Fig. 3C and D). A heatmap of the differential metabolites further illustrated the distinct metabolic patterns between the groups (Supplementary Fig. 3E).

At the superclass level, the differential metabolites were mainly classified as lipids and lipid-like molecules. At the class level, they were primarily enriched in carboxylic acids, their derivatives, and fatty acids (Fig. 2A). Comparative analysis identified 875 differential metabolites between HFCD-HF/G- and JYXZF-treated rats, including 471 upregulated and 404 downregulated metabolites (Supplementary Fig. 3F).

KEGG pathway enrichment analysis showed that these metabolites were mainly associated with amino acid and lipid metabolism, whereas Reactome analysis identified PPAR-regulated lipid metabolic pathways among the most significantly enriched pathways (Fig. 2B and C). Overall, these results suggest that JYXZF reshapes systemic lipid metabolism and may exert its therapeutic effects through modulation of PPAR-linked lipid metabolic pathways in MASLD.

Integrated transcriptomic and metabolomic analyses prioritize a PPARγ/SCD1-related lipid metabolic program associated with JYXZF treatment

To further elucidate the molecular mechanisms through which JYXZF ameliorates hepatic steatosis, we performed hepatic transcriptomic profiling in MASH rats with or without JYXZF and integrated the transcriptomic and serum metabolomic data using WGCNA. PCA of the transcriptomic data showed clear separation between the MASH group and the JYXZF-treated group (Supplementary Fig. 4A). Differential expression analysis ($q < 0.05$, $|\log2FC| > 1.0$) identified 438 DEGs, including 260 upregulated and 178 downregulated genes. Heatmap analysis further revealed distinct gene expression patterns between the two groups (Supplementary Fig. 4B and C). GO, KEGG, Reactome, and WikiPathways enrichment analyses showed that these DEGs were predominantly associated with lipid metabolism, particularly fatty acid biosynthesis and the PPAR signaling pathway. Key genes included PPARγ, SCD1, carnitine palmitoyltransferase 1A (CPT1A), and several fatty acid-binding protein (FABP) family members (Fig. 2D–F). When we applied a less stringent threshold ($|\log2FC| > 0.585$), we identified additional genes within these pathways (Supplementary Fig. 4E–J), further highlighting their central role.

To explore the relationship between the transcriptome and metabolome, WGCNA identified eight gene co-expression modules. Among them, the blue module exhibited the strongest correlation with metabolic traits (Supplementary Fig. 5A and B). We selected core genes within this module ($kME > 0.8$), and their associations with the top 50 metabolites were visualized in a metabolite-module heatmap (Supplementary Fig. 5C). Venn analysis of (i) the 50 metabolites with the highest absolute correlation coefficients, (ii) the 189 metabolites within the blue module, and (iii) the 73 metabolites associated with machine learning-derived core targets identified six key differential metabolites (Supplementary Fig. 5D and E), including eicosatetraenoic acid (Supplementary Fig. 5F), which mapped to PPAR-regulated lipid metabolic pathways (Fig. 2G).

Taken together, the integrated metabolomic and transcriptomic analyses suggest that the PPARγ/SCD1 lipid metabolic program represents an important regulatory pathway within the broader molecular response to JYXZF.

Multi-database integrated network pharmacology and metabolomics identify key targets of JYXZF in MASLD

To investigate the potential molecular mechanisms through which JYXZF acts in MASLD, we integrated multi-database network pharmacology with serum metabolomic data. MA-

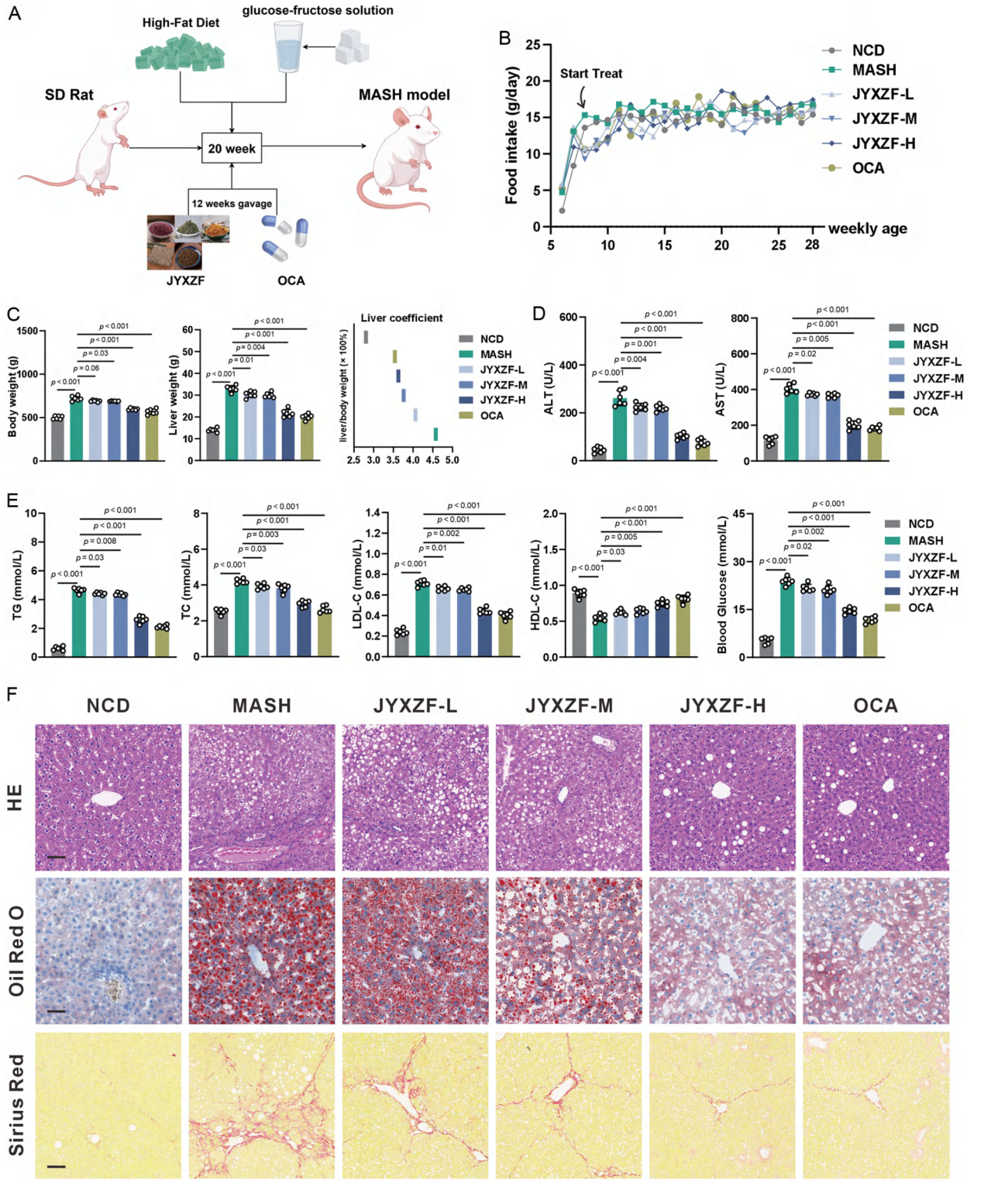

Fig. 1. Metabolic, biochemical, and histological measurements in the MASH rat model. (A) Schematic diagram of SD rat treatment. Eight-week-old rats (n = 6) were fed a MASH diet and then received intragastric administration of low-, medium-, and high-dose JYXZF or OCA for 12 weeks. (B) Changes in food intake of rats in each group. (C) Body weight, liver weight, and liver coefficient (ratio of liver weight/body weight) of rats in each group. (D, E) ALT, AST, TG, TC, LDL-C, HDL-C, and blood glucose levels of rats in each group. (F) Representative images of H&E, Oil Red O staining, and Sirius Red staining of liver sections. Scale bar = 50 μm. Data are presented as mean ± standard deviation. ALT, alanine aminotransferase; AST, aspartate aminotransferase; H&E, hematoxylin and eosin; HDL-C, high-density lipoprotein cholesterol; JYXZF, Juanyu-Xiaozhi Formula; LDL-C, low-density lipoprotein cholesterol; MASH, metabolic dysfunction-associated steatohepatitis; OCA, obeticholic acid; SD, Sprague–Dawley; TC, total cholesterol; TG, triglycerides.

SLD-related targets were collected from OMIM, GeneCards, DisGeNET, and TTD, yielding 22,788 unique disease-associated genes after deduplication. We searched the five herbal components of JYXZF against HERB and TCMSP and identified 900 compound-related targets (Supplementary Table 1). Intersection analysis identified 708 targets shared between JYXZF and MASLD, representing potential therapeutic targets (Supplementary Fig. 6A; Supplementary Table 2).

GO enrichment analysis indicated that these 708 targets were mainly associated with biological processes involved in lipid responses (Supplementary Fig. 6B), whereas KEGG and Reactome analyses showed significant enrichment of lipid metabolism and atherosclerosis-related pathways (Supplementary Fig. 6C and D). We constructed a PPI network using STRING and visualized it in Cytoscape (Supplementary Fig. 6E). Topological analysis based on degree centrality identified 66 key targets using a threshold equal to half of the maximal degree value (Supplementary Table 3).

Next, we constructed a compound-target-pathway network that integrated the 708 genes with their corresponding compounds, and we ranked 150 top-scoring targets according to degree (Supplementary Fig. 6F; Supplementary Table 4). Additionally, 141 level-1 and 228 level-2 metabolites (retention time ± 0.3 min) were matched to SMILES structures through PubChem, and their oral bioavailability was predicted using SwissADME. SwissTargetPrediction yielded 999 putative targets for these metabolites (Supplementary Table 5).

A Venn diagram integrating the PPI key nodes (n = 66), the top-ranked nodes in the compound–target–pathway network (n = 150), and metabolomics-predicted targets (n = 999) identified 44 overlapping targets as key candidate mediators of the therapeutic effects of JYXZF in MASLD (Supplementary Fig. 6G).

Machine learning-assisted prioritization of candidate transcriptomic targets

To prioritize the most relevant targets among the 44 candidates, we analyzed the hepatic transcriptomic data using three machine learning algorithms: LASSO regression, SVM, and artificial neural networks. The dataset was randomly divided into training and validation sets at a 7:3 ratio. Each algorithm selected the top 10 weighted targets according to feature importance (Fig. 3A). Comparison of the results from the three algorithms identified six overlapping targets: PPARα, PPARγ, JUN, FOS, mitogen-activated protein kinase 1 (MAPK1), and histone deacetylase 1 (HDAC1) (Fig. 3G).

Residual plots, the LASSO learning curve, and breakdown/SHAP-based interpretation were used to evaluate the internal stability and interpretability of the candidate ranking within the discovery dataset (Fig. 3B–D). Accumulated dependence profiles illustrated the influence of changes in candidate gene expression on model-derived prioritization. Together with cross-model comparison, these analyses demonstrated consistent effects for PPARα, PPARγ, JUN, FOS, HDAC1, and MAPK1 across the three algorithms (Fig. 3E and F). Correlation analysis also revealed strong associations among PPARα, PPARγ, JUN, and FOS (Fig. 3H).

Integrating the machine learning-prioritized candidates with transcriptomic DEGs showed that PPARγ, JUN, and FOS were not only selected by the algorithms but were also significantly dysregulated after JYXZF treatment (Fig. 3I). As independent transcriptomic datasets from JYXZF-treated models were not available, we used external GEO datasets from MASLD models to validate these findings. Across six GEO datasets, PPARγ, JUN, and FOS showed consistent upregulation in MASLD models compared with normal controls (Fig. 3J). Thus, machine learning provided an independent layer of prioritization, refined conventional multi-omics candidates, and highlighted PPARγ, JUN, and FOS for subsequent functional validation.

Molecular docking and molecular dynamics simulation

To explore the structural basis of JYXZF activity, we scored circulating constituents based on their m/z values and MS/MS fragment patterns. We selected high-scoring compounds from the major structural categories as candidate ligands (Supplementary Table 6). Docking simulations were then performed using PPARγ and AP-1 (JUN/FOS dimer) as representative receptors, based on the multi-omics and machine learning analyses. We retrieved their three-dimensional structures (PDB IDs: 8ATY for PPARγ and 1FOS for AP-1) from the RCSB Protein Data Bank.

Molecular docking showed that several JYXZF-derived flavonoids and related small molecules formed stable interactions with both PPARγ and AP-1 (Fig. 4A). Nepetin showed the strongest binding affinity for PPARγ and interacted with residues SER289, GLU295, and LYS367, whereas luteolin-7-glucuronide interacted with LEU228, TYR327, and LYS367 in PPARγ and with ARG159, ARG285, and ARG288 in AP-1. Other circulating compounds, including hispidulin-7-glucuronide and rutin, also exhibited appreciable affinity for both PPARγ and AP-1, with binding energies ranging from −4.6 to −10.7 kcal/mol (Supplementary Table 7).

To evaluate the stability of the docking results, molecular dynamics simulations were conducted on representative flavonoid-PPARγ/AP-1 complexes. RMSD reached equilibrium at approximately 20 ns and remained stable throughout the 100-ns simulation, indicating conformational stability (Fig. 4B). The center-of-mass distance between the ligand and the binding pocket fluctuated only within a narrow range (0.6–0.8 nm), suggesting persistent ligand residence (Supplementary Fig. 7A). Rg values remained between 2.65 and 2.75 nm with minimal fluctuation (Supplementary Fig. 7B), indicating that the global protein structure remained compact. Finally, RMSF analysis showed limited local flexibility (0.1–0.25 nm for most residues), with particularly low mobility at binding-site residues, consistent with stable ligand binding (Supplementary Fig. 7C).

These docking and molecular dynamics results suggest that selected circulating constituents of JYXZF likely interact with PPARγ and AP-1, supporting target prioritization.

AP-1 participates in JYXZF-mediated suppression of PPARγ/SCD1-related signaling

To validate the expression changes in the core genes identified above, we first examined liver tissues from normal chow diet (NCD), MASH, and JYXZF-treated rats. Western blot analysis showed that FOS, JUN, and PPARγ were upregulated in the MASH group compared with the NCD control group, whereas JYXZF treatment substantially reduced their protein levels (Fig. 5A). Consistent with the transcriptomic results, RT-qPCR analysis revealed that multiple PPARγ pathway-related genes were downregulated after JYXZF treatment, with SCD1 showing one of the most prominent decreases (Fig. 5B). Additionally, JYXZF-medicated serum reduced the protein and mRNA expression of FOS, JUN, PPARγ, and SCD1 in FFA-induced steatotic HepG2 cells, consistent with the *in vivo* findings (Supplementary Fig. 8A and B).

Given that the AP-1 complex (c-Jun/c-Fos dimers) is known to enhance PPARγ promoter activity and thereby increase PPARγ expression,[54] we hypothesized that AP-1 modulation may contribute to the inhibitory effect of JYXZF on PPARγ signaling. To test this, a luciferase reporter assay was

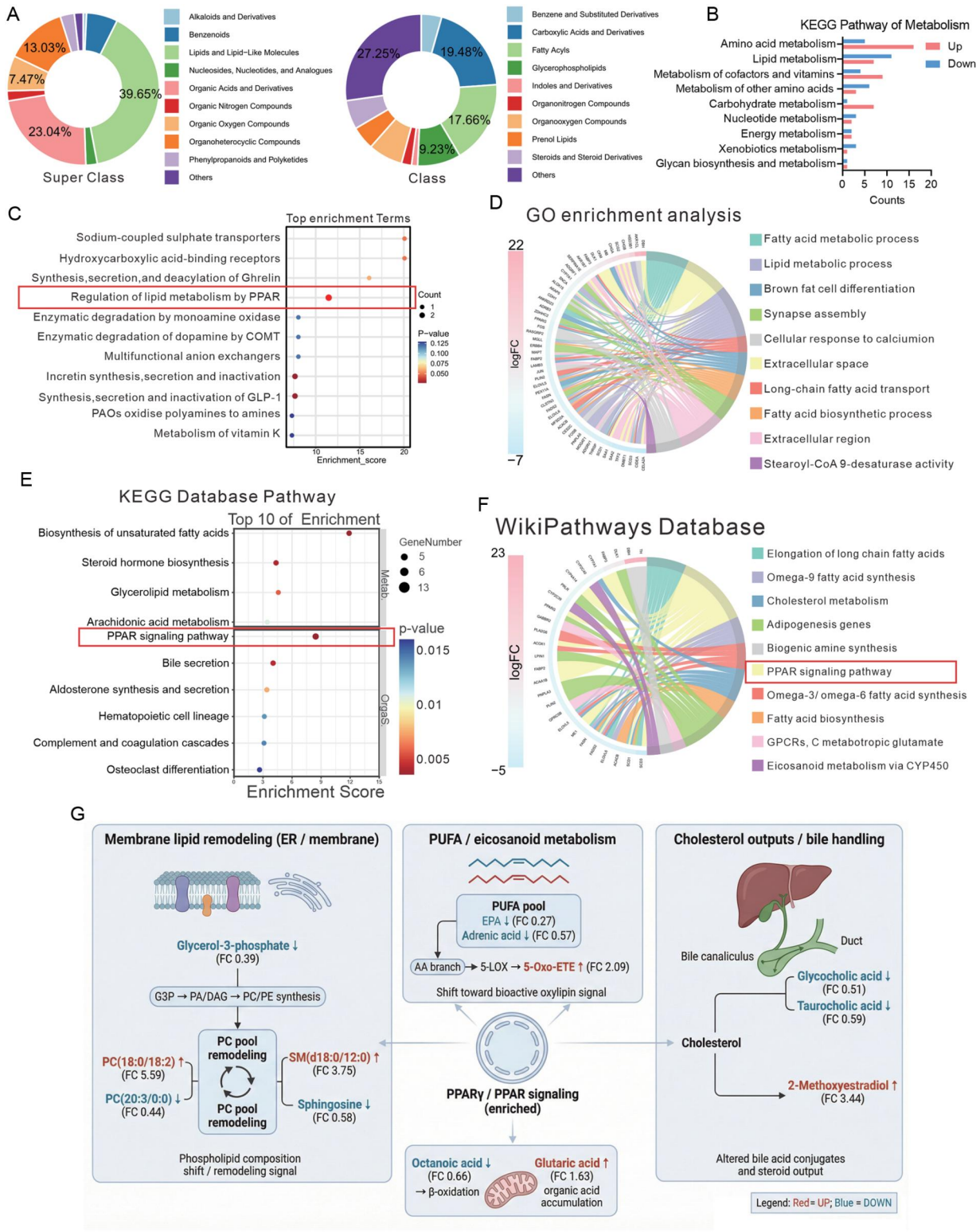

Fig. 2. Metabolomics and transcriptomics profiling of the liver from the MASH group and the JYXZF-treated group. (A) Classification of differential metabolites by superclass and class. (B) KEGG metabolic pathway enrichment analysis of differential metabolites. (C) Reactome database pathway enrichment analysis of differential metabolites. (D) GO enrichment analysis of DEGs from the MASH group versus the optimal-dose JYXZF treatment group. (E) KEGG pathway enrichment analysis of DEGs. (F) WikiPathways analysis of DEGs. (G) Integrated transcriptomic and metabolomic analysis showing pathway enrichment of differential metabolites. CYP450, Cytochrome P450; DEGs, differentially expressed genes; GO, Gene Ontology; GPCRs, G-protein-coupled receptors; JYXZF, Juanyu-Xiaozhi Formula; PUFA, polyunsaturated fatty acid; PPAR, peroxisome proliferator-activated receptor; KEGG, Kyoto Encyclopedia of Genes and Genomes; MASH, metabolic dysfunction-associated steatohepatitis.

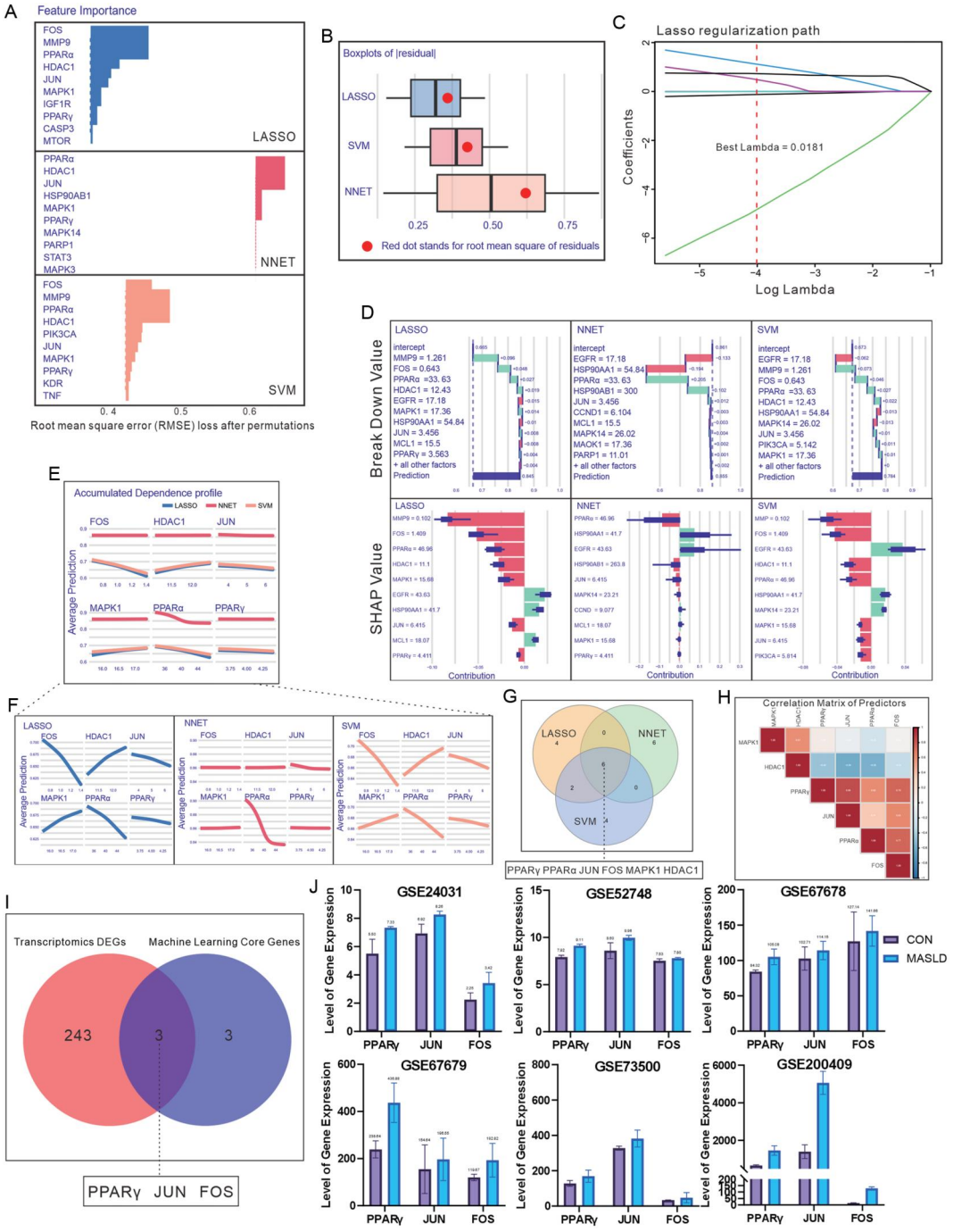

Fig. 3. Machine-learning-assisted prioritization and external disease-context assessment of candidate transcriptomic targets. (A) Feature importance evaluation of key genes using three machine learning models based on the transcriptomic training dataset. (B) Boxplot of residual absolute errors across models; red dots indicate RMSE. (C) LASSO regression learning curve. (D) Validation of gene importance using the validation dataset by the Break Down Method and SHAP values. (E, F) ADPs of core targets and comparative changes in core targets across three models, yielding six core genes. (G) Intersection of the top 10 important genes among the three models, yielding six core genes. (H) Correlation analysis of the six core genes in the transcriptomic data. (I) Overlap of core genes with transcriptomic DEGs (fold change > 2.0). (J) External validation using GEO datasets (GSE24031, GSE52748, GSE67678, GSE67679, GSE73500, GSE200409); all datasets were selected from normal diet-fed controls (Con) and MASLD. ADP, accumulated dependence profile; CASP3, caspase 3; Con, normal control; DEGs, differentially expressed genes; FOS, Fos proto-oncogene; GEO, Gene Expression Omnibus; HDAC1, histone deacetylase 1; HSP90AB1, heat shock protein 90 alpha family class B member 1; IGF1R, insulin-like growth factor 1 receptor; JUN, Jun proto-oncogene; KDR, kinase insert domain receptor; LASSO, least absolute shrinkage and selection operator; MAPK1, mitogen-activated protein kinase 1; MAPK3, mitogen-activated protein kinase 3; MAPK14, mitogen-activated protein kinase 14; MASLD, metabolic dysfunction-associated steatotic liver disease; MMP9, matrix metallopeptidase 9; MTOR, mechanistic target of rapamycin kinase; NNET, neural network; PARP1, poly(ADP-ribose) polymerase 1; PIK3CA, phosphatidylinositol-4,5-bisphosphate 3-kinase catalytic subunit alpha; PPARα, peroxisome proliferator-activated receptor alpha; PPARγ, peroxisome proliferator-activated receptor gamma; RMSE, root mean square error; SHAP, SHapley Additive exPlanations; STAT3, signal transducer and activator of transcription 3; SVM, support vector machine; TNF, tumor necrosis factor.

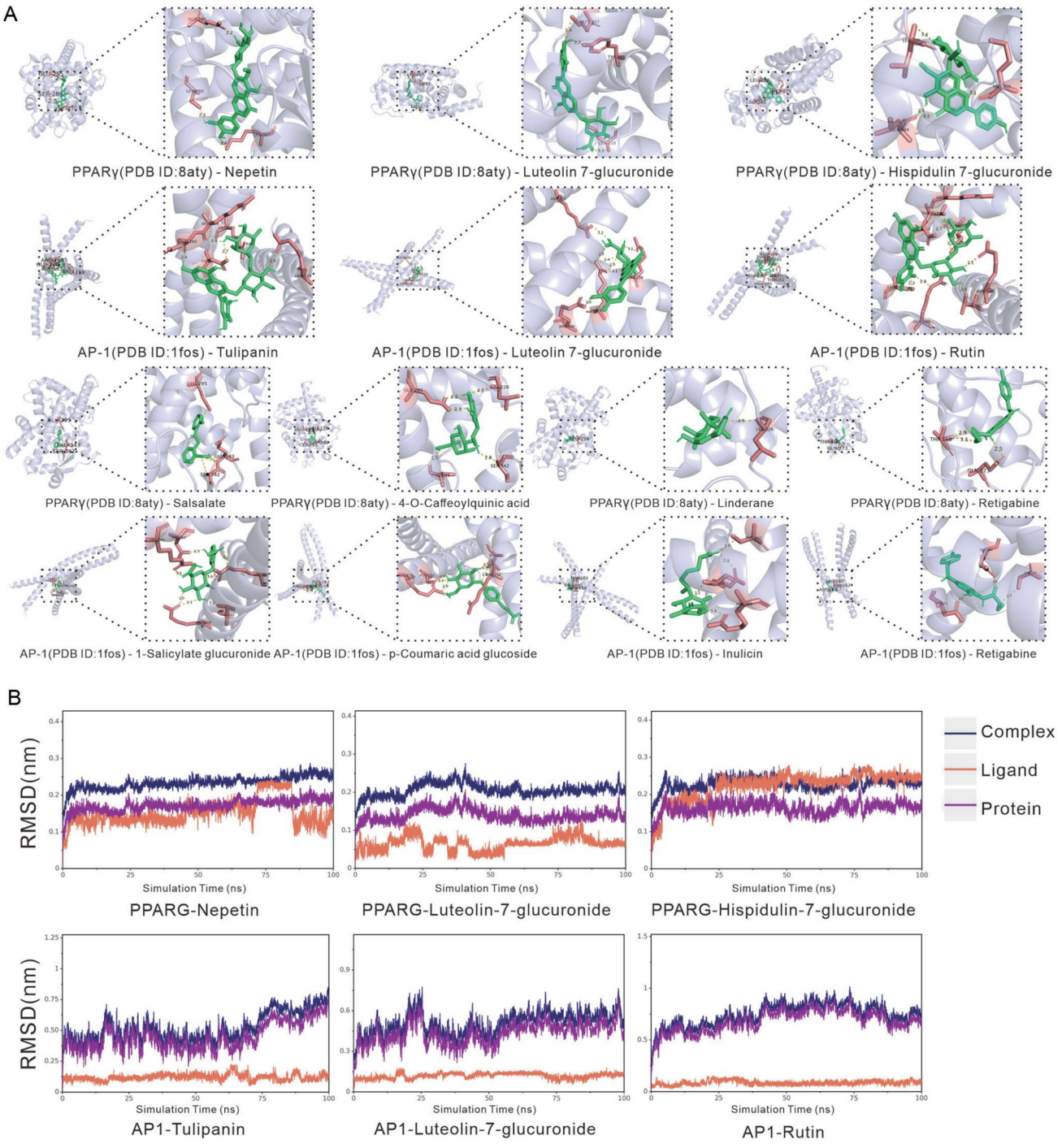

Fig. 4. Molecular docking and molecular dynamics analyses of representative circulating JYXZF constituents with selected protein structures. (A) Molecular docking results for three major flavonoids and four minor compounds against core targets. (B) Molecular dynamics simulation trajectories and binding stability for flavonoid-target complexes (RMSD curves). AP-1, activator protein 1; JYXZF, Juanyu-Xiaozhi Formula; RMSD, root-mean-square deviation; PPAR, peroxisome proliferator-activated receptor.

performed using constructs containing the PPARγ promoter. JYXZF treatment reduced PPARγ promoter activity, whereas AP-1 overexpression (OE-AP-1) significantly reversed the inhibitory effect of JYXZF (Fig. 5C). To further assess AP-1 binding to the PPARγ promoter, we performed ChIP-qPCR to measure c-Jun/c-Fos binding to the AP-1 motif within the PPARγ promoter. In FFA-treated HepG2 cells, AP-1 occupancy at the PPARγ promoter was significantly increased relative to control cells, whereas JYXZF treatment substantially reduced this occupancy. Pharmacological AP-1 inhibition with T-5224 produced a similar decrease in AP-1 binding (Supplementary Fig. 8C). Conversely, phorbol 12-myristate 13-acetate (PMA)-

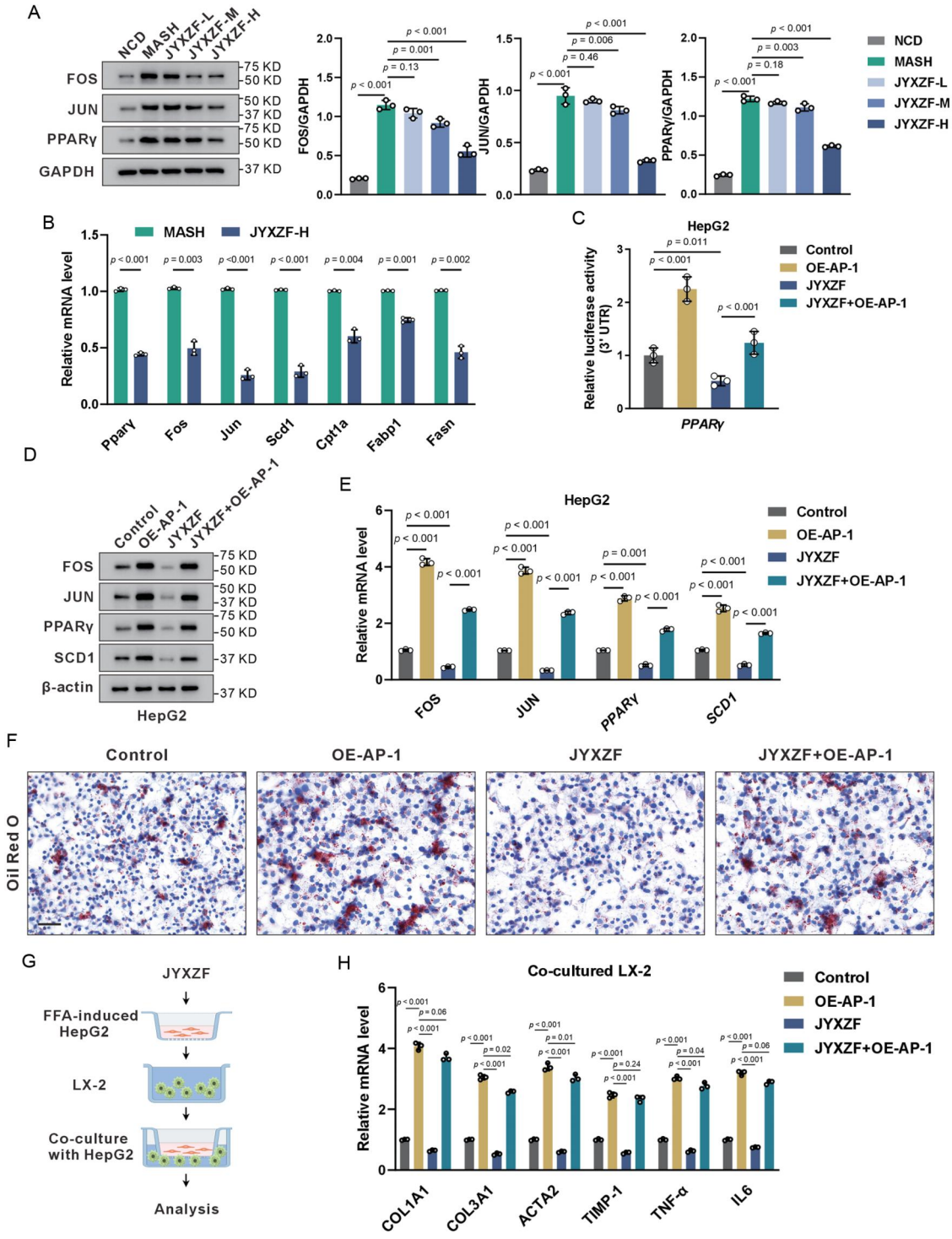

Fig. 5. AP-1 modulation and PPARγ/SCD1-related measurements in liver tissues and FFA-induced HepG2 cells. (A) Western blot analysis of FOS, JUN, and PPARγ expression in liver tissues from the NCD, MASH, and JYXZF-treated groups. (B) Analysis of PPARγ signaling pathway-related gene expression in the livers of MASH and JYXZF-H groups by RT-qPCR. (C–F) HepG2 cells were first incubated with 0.5 mM FFA for 12 h and then subjected to AP-1 overexpression (AdFOS and AdJUN), JYXZF treatment, or combined JYXZF treatment and AP-1 overexpression. (C) Relative luciferase activity of reporter constructs containing the PPARγ promoter region (n = 3). (D–E) Protein and relative mRNA levels (n = 3) of FOS, JUN, PPARγ, and SCD1 were determined by western blotting and RT-qPCR. (F) Representative images of Oil Red O staining. Scale bar = 50 μm. (G, H) LX-2 cells were co-cultured with FFA-induced HepG2 cells (treated as described above). The indicated mRNA levels of LX-2 cells were analyzed by RT-qPCR (n = 3, performed in triplicate). Data are presented as mean ± standard deviation. AP-1, activator protein 1; FFA, free fatty acid; FOS, Fos proto-oncogene; H&E, hematoxylin and eosin; HepG2, human hepatocellular carcinoma cell line HepG2; JYXZF, Juanyu-Xiaozhi Formula; JUN, Jun proto-oncogene; LX-2, human hepatic stellate cell line; MASH, metabolic dysfunction-associated steatohepatitis; NCD, normal chow diet; PPARγ, peroxisome proliferator-activated receptor gamma; RT-qPCR, reverse transcription quantitative polymerase chain reaction; SCD1, stearoyl-CoA desaturase 1.

induced AP-1 activation further enhanced promoter binding, and co-treatment with JYXZF partially attenuated this effect (Supplementary Fig. 8D). In parallel, AP-1 overexpression largely restored the protein and mRNA levels of FOS, JUN, PPARγ, and SCD1 that had been decreased by JYXZF in FFA-treated HepG2 cells (Fig. 5D and E). Functionally, Oil Red O staining and co-culture experiments demonstrated that AP-1 overexpression largely counteracted the inhibitory effects of JYXZF on hepatic lipid accumulation and HSC activation *in vitro* (Fig. 5F–H).

To further examine the contribution of AP-1 to PPARγ/SCD1-related signaling, we performed AP-1 loss-of-function experiments using siRNA-mediated knockdown of JUN and FOS. Compared with the control group, knockdown of AP-1 significantly reduced both PPARγ expression and lipid accumulation. Moreover, combined treatment with JYXZF exerted an inhibitory effect similar to that of the AP-1 knockdown group alone, suggesting that AP-1 is a functionally relevant contributor to JYXZF-induced downregulation of PPARγ. The combined treatment exhibited a stronger lipid-lowering effect than AP-1 knockdown alone, indicating that additional AP-1-independent mechanisms may also contribute to the anti-steatotic effects of JYXZF. This finding is consistent with its multicomponent pharmacological characteristics (Supplementary Fig. 8E and F).

Collectively, these data support the involvement of AP-1-dependent transcriptional regulation of PPARγ in the response to JYXZF.

SCD1 perturbation supports its functional involvement in JYXZF-regulated lipid metabolism

Given that SCD1 is an important lipogenic gene downstream of PPARγ signaling, we next investigated whether manipulating SCD1 would affect the therapeutic effects of JYXZF in MASLD. We established a liver-specific AAV-*Scd1* overexpression model and treated the MASH rat model with JYXZF (Fig. 6A and B). JYXZF alone significantly reduced body weight, liver weight, and the liver-to-body weight ratio compared with the MASH group, whereas AAV-*Scd1* largely abolished these improvements (Fig. 6C). Consistently, JYXZF lowered blood glucose and improved serum lipid profiles, liver enzyme profiles, and inflammatory markers (ALT, AST, TG, TC, LDL, HDL, TNF-α, and IL-6), whereas AAV-*Scd1* largely abolished these metabolic benefits (Fig. 6D–F). Histological assessment further showed that AAV-*Scd1* substantially counteracted the JYXZF-induced reduction in hepatic steatosis and fibrosis, resulting in greater hepatic lipid and collagen deposition compared with JYXZF alone (Fig. 6G). Further *in vitro* validation demonstrated that SCD1 overexpression significantly compromised the suppressive effects of JYXZF on hepatic steatosis and HSC activation (Supplementary Fig. 9A–D).

Collectively, both *in vivo* and *in vitro* gain-of-function experiments showed that SCD1 overexpression substantially attenuated the ability of JYXZF to reduce hepatic lipid accumulation, metabolic disturbances, inflammatory responses, and fibrotic alterations. These findings support SCD1 as a functionally important downstream mediator of JYXZF-regulated lipid metabolic remodeling.

Purified circulating flavonoids contribute to the anti-steatotic activity of JYXZF

Four abundant circulating constituents, luteolin-7-glucuronide, nepetin, hispidulin-7-glucuronide, and rutin, were confirmed by targeted UPLC-MS/MS (Fig. 7A). The mass spectra and corresponding m/z values for the four circulating constituents of JYXZF are shown in Figure 7B. To determine whether these circulating constituents contributed to the anti-steatotic effect, FFA-induced HepG2 cells were treated with JYXZF-medicated serum, used as a surrogate for the active circulating small-molecule mixture; purified monomers; the four-compound mixture; or OCA. CCK-8 assays showed that the four-compound mixture (LNHR) at concentrations up to 20% (v/v) had little effect on cell viability, whereas higher concentrations (30–50%) significantly reduced viability (Fig. 7C). Therefore, we selected 20% as the working concentration. We then treated FFA-induced HepG2 cells with each purified monomer, the four-compound mixture, or JYXZF-medicated serum. Compared with the FFA group, TG and TC levels in the culture supernatant were significantly decreased across all treatment groups. In particular, the LNHR group showed markedly reduced TG and TC levels, with an effect comparable to that of the JYXZF-medicated serum group (Fig. 7D). Consistently, Oil Red O staining corroborated these findings and showed that the four-compound mixture and JYXZF-medicated serum markedly reduced FFA-induced lipid droplet accumulation in HepG2 cells (Fig. 7E). These findings indicate that four key circulating constituents of JYXZF attenuate hepatic steatosis *in vitro*, with efficacy comparable to that of JYXZF-medicated serum. Additionally, the four purified monomers reduced lipid deposition to different extents. Among the individual monomers, rutin exhibited the strongest anti-steatotic effect, followed by luteolin-7-glucuronide, nepetin, and hispidulin-7-glucuronide. Notably, the optimized four-compound mixture exhibited a stronger lipid-lowering effect than any single monomer and was second only to JYXZF-medicated serum.

Discussion

MASLD is characterized by metabolic dysregulation, hepatic lipid accumulation, inflammation, and fibrotic remodeling, yet effective therapeutic options remain limited.[55–57] Although TCM formulas have shown beneficial effects in fatty liver disease, previous studies have often focused on phenotypic improvement, network pharmacology analyses, or pathway enrichment, leaving the circulating bioactive constituents and functionally relevant mechanisms insufficiently characterized. In this study, we integrated UPLC-MS/MS-based circulating constituent profiling, serum metabolomics, hepatic transcriptomics, network pharmacology, machine learning-assisted target prioritization, and functional perturbation experiments. This approach established a framework that links JYXZF constituents to MASLD-related regulatory pathways. These findings suggest that the AP-1/PPARγ/SCD1-related lipid metabolic pathway contributes to the therapeutic effects of JYXZF (Fig. 8).

Identification of circulating constituents provides an important pharmacological link between chemical profiling and biological activity.[58] Among the circulating compounds detected after JYXZF administration, flavonoid-related constituents, including nepetin, luteolin-7-glucuronide, hispidulin-7-glucuronide, and rutin, were prominent. These compounds have been reported to exert anti-inflammatory, antioxidant, insulin-sensitizing, and lipid-regulatory activities, suggesting their potential roles in metabolic and inflammatory disorders.[59–62] In this study, experimental validation of the purified compounds further showed that these representative flavonoids reduced lipid accumulation to different extents in FFA-induced HepG2 cells. Importantly, their combination exerted a stronger anti-steatotic effect than any single compound. However, the mixture did not fully reproduce the activity of JYXZF-medicated serum, suggesting that these flavonoids are pharmacologically relevant contributors but do

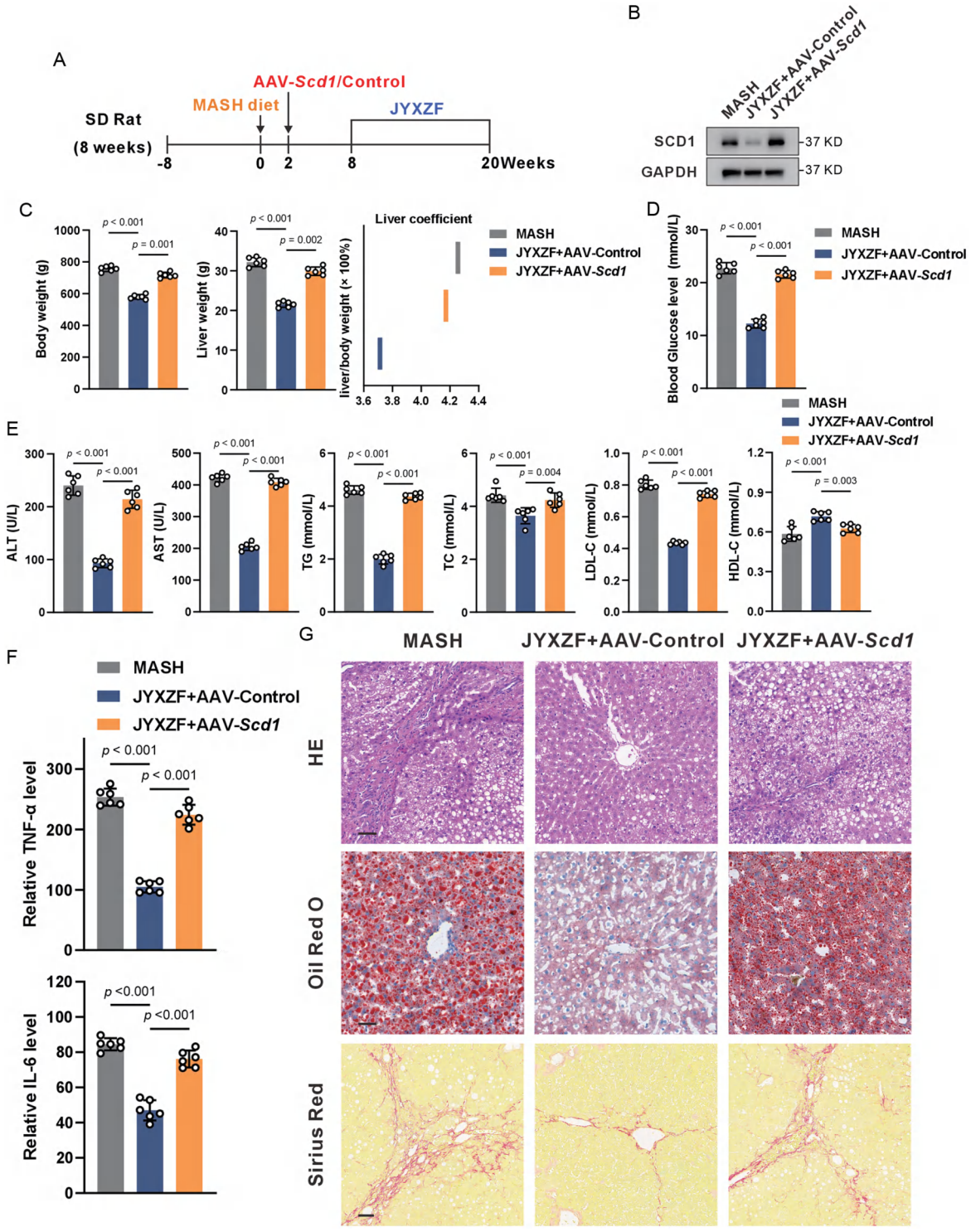

Fig. 6. Metabolic, biochemical, and histological measurements in MASH rats with AAV-mediated *Scd1* overexpression and JYXZF treatment. (A) Schematic diagram of SD rat treatment. Briefly, SD rats (n = 6) were fed a MASH diet and then received liver-specific AAV injections (AAV-control or AAV-*Scd1*) via the tail vein at 10 weeks of age, followed by a 12-week treatment with JYXZF. (B) Analysis of SCD1 expression in the livers of rats by western blot. (C) Body weight, liver weight, and liver coefficient (ratio of liver weight/body weight) of rats in each group. (D) Blood glucose levels of rats in each group. (E) ALT, AST, TG, TC, LDL-C, and HDL-C levels of rats in each group. (F) Relative TNF-α and IL-6 levels in liver tissues. (G) Representative images of H&E, Oil Red O staining, and Sirius Red staining of liver sections. Scale bar = 50 μm. Data are presented as mean ± standard deviation. AAV, adeno-associated virus; ALT, alanine aminotransferase; AST, aspartate aminotransferase; HDL-C, high-density lipoprotein cholesterol; H&E, hematoxylin and eosin; IL-6, interleukin-6; JYXZF, Juanyu-Xiaozhi Formula; LDL-C, low-density lipoprotein cholesterol; MASH, metabolic dysfunction-associated steatohepatitis; Scd1, stearoyl-CoA desaturase 1; SD, Sprague–Dawley; TC, total cholesterol; TG, triglycerides; TNF-α, tumor necrosis factor alpha.

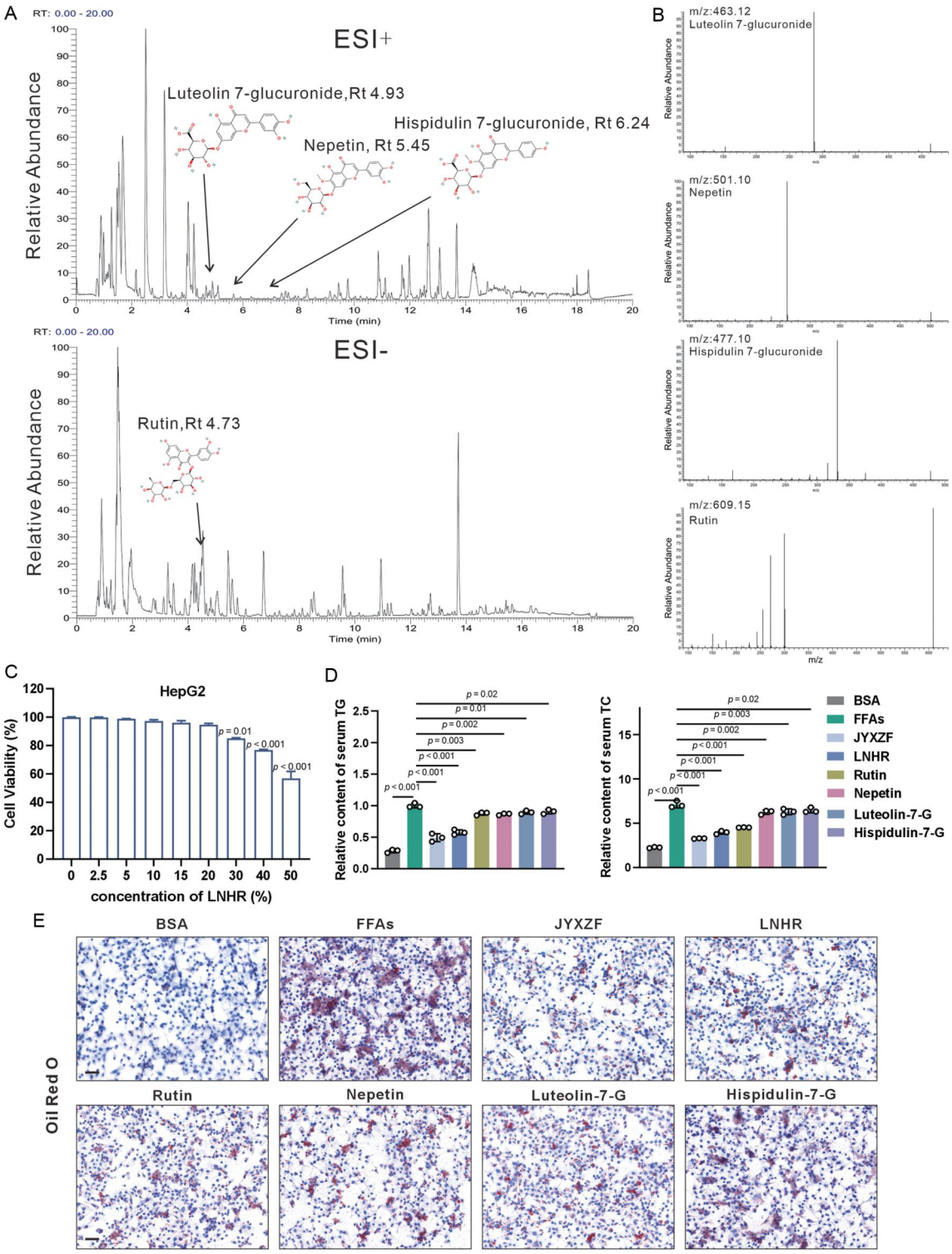

Fig. 7. UPLC-MS/MS identification of circulating JYXZF constituents and *in vitro* measurements after treatment with key compounds in FFA-induced HepG2 cells. (A) UPLC-MS/MS analysis of the four representative circulating constituents of JYXZF. (B) Mass spectra and m/z information for four key active constituents of JYXZF circulating in blood. (C–E) HepG2 cells were incubated with 0.5 mM FFA for 24 h and then treated with each purified monomer, a low- or high-concentration four-compound mixture (LNHR), or JYXZF-medicated serum. (C) Cell viability after treatment with different concentrations of LNHR. (D) TG and TC levels in the culture supernatant after the indicated treatments in each group (n = 3). (E) Representative images of Oil Red O staining in each group. Scale bar = 50 μm. Data are presented as mean ± standard deviation. CCK-8, Cell Counting Kit-8; FFA, free fatty acid; HepG2, human hepatocellular carcinoma cell line HepG2; JYXZF, Juanyu-Xiaozhi Formula; LNHR, luteolin-7-glucuronide, nepetin, hispidulin-7-glucuronide, and rutin; m/z, mass-to-charge ratio; TC, total cholesterol; TG, triglycerides; UPLC-MS/MS, ultra-high-performance liquid chromatography–tandem mass spectrometry.

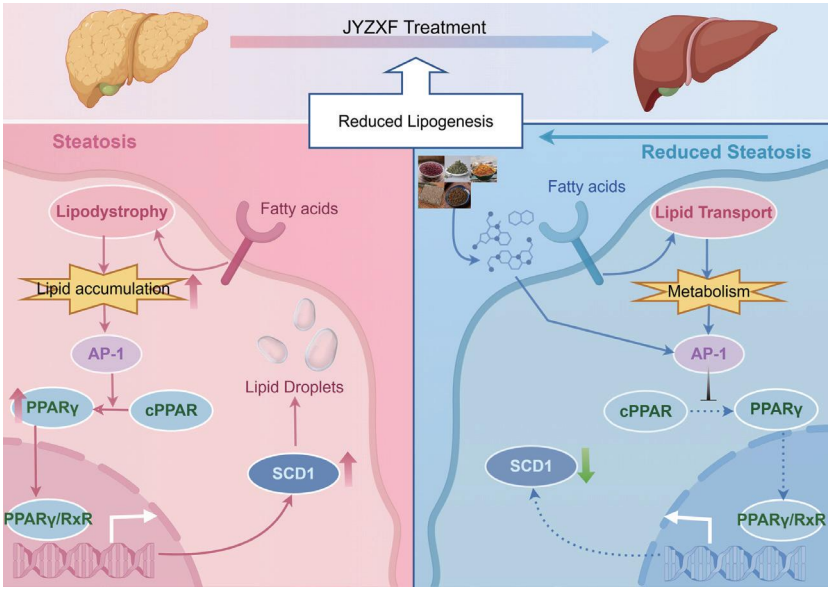

Fig. 8. Schematic diagram of the molecular mechanism of JYXZF in treating MASLD. AP-1, activator protein-1; PPARγ, peroxisome proliferator-activated receptor gamma; cPPAR, competing peroxisome proliferator-pctivated preceptor; SCD1, stearoyl-CoA desaturase 1; RXR, retinoid X receptor heterodimer; JYXZF, Juanyu-Xiaozhi formula; MASLD, metabolic dysfunction-associated steatotic liver disease.

not fully account for the effects of the whole formula. Other circulating metabolites, non-flavonoid constituents, and interactions between multiple chemical classes may also have contributed to the overall efficacy of JYXZF.

PPARγ is an important nuclear receptor involved in lipid metabolism, fatty acid handling, and hepatic steatosis.[63,64] In hepatocytes, excessive PPARγ activation promotes triglyceride synthesis and lipid droplet formation partly through lipogenic genes such as SCD1, which facilitates the conversion of saturated fatty acids into monounsaturated fatty acids and promotes lipid synthesis and storage.[65] Given the established roles of AP-1 in metabolic inflammation and lipid regulation,[54] our findings suggest that AP-1 inhibition may contribute to reduced PPARγ-driven lipogenic signaling and SCD1-associated lipid accumulation. Functional perturbation experiments further supported the role of SCD1 as a downstream mediator of this lipid-regulatory response. Nevertheless, considering the multicomponent nature of JYXZF and the complexity of MASLD pathogenesis, the AP-1/PPARγ/SCD1 axis should be viewed as an important validated mechanism within the broader multi-target actions of JYXZF, rather than as an exclusive or fully resolved causal cascade.

Compared with other TCM formulas studied for fatty liver disease, JYXZF showed both shared and distinct mechanisms. Xiaoyaosan has been reported to improve hepatic steatosis, oxidative stress, inflammation, and metabolic dysregulation through pathways identified by multi-omics approaches.[66] Yinchenhao Tang has been more closely associated with bile acid metabolism, farnesoid X receptor (FXR)-related regulation, and reduced HSC activation through TGF-β/Smad/extracellular regulated protein kinase (ERK) signaling.[22,67] JYXZF shares the multicomponent and multi-target characteristics of these formulas. However, the present study provides evidence that JYXZF may act through a distinct pathway centered on circulating flavonoid-related constituents and AP-1/PPARγ/SCD1-mediated lipid regulation. This comparison suggests that different TCM formulas may improve similar metabolic and inflammatory phenotypes through partially distinct molecular networks.

From a translational perspective, JYXZF may represent a multicomponent metabolic intervention for MASLD phenotypes characterized by steatosis, inflammation, insulin resistance, and early fibrotic changes. Current MASH drug development has largely focused on pathway-selective agents, including FXR agonists, THR-β agonists,[68] PPAR agonists, and incretin-based therapies. Resmetirome was approved by the FDA in 2024 for adults with noncirrhotic MASH and moderate-to-advanced fibrosis. However, its indication remains focused on a specific patient subgroup.[69] Although OCA, an FXR agonist, has shown antifibrotic potential in MASH studies,[70] its development for MASH has been limited by regulatory and safety concerns, and it is not currently approved for MASH treatment.[71] In contrast to these pathway-selective strategies, JYXZF improved hepatic steatosis, lipid metabolism, insulin sensitivity, inflammation, and collagen deposition in a diet-induced MASH model. These findings suggest a broader multi-target regulatory profile for JYXZF. Therefore, the use of JYXZF may serve as a complementary or alternative strategy for the treatment of metabolically driven MASLD. Moreover, identifying active constituents and key targets provides a basis for standardized formula development, active-compound-guided target optimization, and future small-molecule discovery targeting lipid-regulatory pathways such as AP-1/PPARγ/SCD1. A feasible next step would be a randomized, double-blind, placebo-controlled pilot trial evaluating standardized JYXZF as an adjunct to lifestyle intervention in patients with metabolically driven MASLD/MASH.[72,73]

This study has a few limitations. First, although representative circulating flavonoids have been validated *in vitro*, the quantitative contribution of each compound to the whole formula effect remains unclear. Future studies using constituent depletion, enrichment, or defined compound combinations are required to determine the relative pharmacological contributions. Second, pathway validation mainly focused on the AP-1/PPARγ/SCD1-related network, whereas other compound classes in JYXZF, including terpenoids and polysaccharides, may act through AP-1-independent mechanisms

such as AMPK-mediated metabolic regulation, G protein-coupled receptor (GPCR) signaling, bile acid metabolism, or immune modulation. Third, although ChIP-qPCR and promoter-reporter assays supported AP-1-dependent regulation of PPARγ, additional *in vivo* genetic models would further strengthen causal inference. Finally, although AAV-mediated SCD1 overexpression supported its functional contribution to the lipid-lowering effects of JYXZF, further studies with SCD1-specific knockout models are needed to clarify its critical role in this process.

Conclusions

This study demonstrates the therapeutic efficacy of JYXZF in a MASH diet-induced rat model and elucidates its lipid-lowering and antifibrotic mechanisms through an integrated strategy combining multi-omics analyses, machine learning-based target prioritization, and functional validation experiments. We further show that JYXZF reduces hepatic lipid accumulation and collagen deposition by attenuating AP-1-mediated transcriptional activation of PPARγ and its downstream effector SCD1. Regulation of this AP-1/PPARγ/SCD1 pathway may contribute to the protective effects of JYXZF against MASLD/MASH progression. These findings not only clarify the mechanisms underlying the effects of JYXZF but also provide a basis for developing multi-target therapeutic approaches for metabolic liver diseases based on TCM.

Supporting information

Supplementary material for this article is available at https://doi.org/10.14218/JCTH.2026.00106.

Funding

This work was supported by the China National Natural Science Foundation (grant number: 82405162), the Natural Science Foundation Project of Chongqing (grant number: CSTB2024NSCQ-MSX0592), the 2023 Chongqing Postdoctoral Innovation Talent Support Program (grant number: CQBX202310), the Chongqing Medical Young Talents Program (grant number: YXQN202445), the 76th China Postdoctoral Science Fund (grant number: 2024MD764040), the Traditional Chinese Medicine Prevention and Treatment of Liver Fibrosis Innovative Team, the Young Talent Program of the Chongqing Jiangbei Talent Program, the 2025 Special Research Project on Liver Diseases of Beijing Medical Science and Technology Development Society (iGandanF-1082025-LG050), the Remarkable Innovation-Clinical Research Project of The Second Affiliated Hospital of Chongqing Medical University, and the First Batch of Key Disciplines on Public Health in Chongqing, Health Commission of Chongqing, China.

Conflict of interest

The authors have no conflict of interests related to this publication.

Author contributions

Visualization (ZJ, YH), methodology (ZJ, YH), investigation (ZJ, YH, CZ, YZ, YQ), writing-original draft (ZJ), formal analysis (CZ), supervision (YY), conceptualization (YY), funding acquisition (YY), writing-review and editing (HL), and project administration (HL). All authors have approved the final version and publication of the manuscript.

Ethical statement

Animal feeding, care, sample collection, and all experimental procedures were conducted in accordance with relevant institutional guidelines for animal care and use, and were approved by the Ethics Committee of Chongqing Medical University (license number: IACUC-SAHCQMU-2025-0141) and Chongqing Traditional Chinese Medicine Hospital (license number: 2024-DWSY-YY). All animals received humane care throughout the study.

Data sharing statement

The original contributions presented in this study are included in the article/Supplementary Material. Further inquiries are available from the corresponding authors upon reasonable request.

References

[1] Targher G, Byrne CD, Tilg H. MASLD: a systemic metabolic disorder with cardiovascular and malignant complications. Gut 2024;73(4):691–702. doi:10.1136/gutjnl-2023-330595, PMID:38228377.
[2] Wong VW, Ekstedt M, Wong GL, Hagström H. Changing epidemiology, global trends and implications for outcomes of NAFLD. J Hepatol 2023;79(3):842–852. doi:10.1016/j.jhep.2023.04.036, PMID:37169151.
[3] Kendall TJ, Jimenez-Ramos M, Turner F, Ramachandran P, Minnier J, McColgan MD, *et al*. An integrated gene-to-outcome multimodal database for metabolic dysfunction-associated steatotic liver disease. Nat Med 2023;29(11):2939–2953. doi:10.1038/s41591-023-02602-2, PMID:37903863.
[4] Loomba R, Friedman SL, Shulman GI. Mechanisms and disease consequences of nonalcoholic fatty liver disease. Cell 2021;184(10):2537–2564. doi:10.1016/j.cell.2021.04.015, PMID:33989548.
[5] Hu Y, Sun C, Chen Y, Liu YD, Fan JG. Pipeline of New Drug Treatment for Non-alcoholic Fatty Liver Disease/Metabolic Dysfunction-associated Steatotic Liver Disease. J Clin Transl Hepatol 2024;12(9):802–814. doi:10.14218/JCTH.2024.00123, PMID:39280073.
[6] Heeren J, Scheja L. Metabolic-associated fatty liver disease and lipoprotein metabolism. Mol Metab 2021;50:101238. doi:10.1016/j.molmet.2021.101238, PMID:33892169.
[7] Younossi ZM, Zelber-Sagi S, Henry L, Gerber LH. Lifestyle interventions in nonalcoholic fatty liver disease. Nat Rev Gastroenterol Hepatol 2023;20(11):708–722. doi:10.1038/s41575-023-00800-4, PMID:37402873.
[8] Bo T, Gao L, Yao Z, Shao S, Wang X, Proud CG, *et al*. Hepatic selective insulin resistance at the intersection of insulin signaling and metabolic dysfunction-associated steatotic liver disease. Cell Metab 2024;36(5):947–968. doi:10.1016/j.cmet.2024.04.006, PMID:38718757.
[9] Feng X, Zhang R, Yang Z, Zhang K, Xing J. Mechanism of Metabolic Dysfunction-associated Steatotic Liver Disease: Important role of lipid metabolism. J Clin Transl Hepatol 2024;12(9):815–826. doi:10.14218/JCTH.2024.00019, PMID:39280069.
[10] Barb D, Kalavalapalli S, Godinez Leiva E, Bril F, Huot-Marchand P, Dzen L, *et al*. Pan-PPAR agonist lanifibranor improves insulin resistance and hepatic steatosis in patients with T2D and MASLD. J Hepatol 2025;82(6):979–991. doi:10.1016/j.jhep.2024.12.045, PMID:39824443.
[11] Zhang Y, Xu J, Zhou D, Ye T, Zhou P, Liu Z, *et al*. Swimming exercise ameliorates insulin resistance and nonalcoholic fatty liver by negatively regulating PPARγ transcriptional network in mice fed high fat diet. Mol Med 2023;29(1):150. doi:10.1186/s10020-023-00740-4, PMID:37907845.
[12] Zhang LJ, Li SY, Fan SL, Nuerbiye A, Zhao JY, Keremu B, *et al*. Hepatoprotective activity of mulberry extract in NAFLD mice for regulating lipid metabolism and inflammation identified via AMPK/PPAR-γ/NF-κB axis. J Ethnopharmacol 2025;351:120108. doi:10.1016/j.jep.2025.120108, PMID:40490232.
[13] Chen H, Tan H, Wan J, Zeng Y, Wang J, Wang H, *et al*. PPAR-γ signaling in nonalcoholic fatty liver disease: Pathogenesis and therapeutic targets. Pharmacol Ther 2023;245:108391. doi:10.1016/j.pharmthera.2023.108391, PMID:36963510.
[14] Hall JA, Ramachandran D, Roh HC, DiSpirito JR, Belchior T, Zushin PH, *et al*. Obesity-Linked PPARγ S273 Phosphorylation Promotes Insulin Resistance through Growth Differentiation Factor 3. Cell Metab 2020;32(4):665–675.e6. doi:10.1016/j.cmet.2020.08.016, PMID:32941798.
[15] Shang Z, Gao Y, Xue Y, Zhang C, Qiu J, Qian Y, *et al*. Shenge Formula attenuates high-fat diet-induced obesity and fatty liver via inhibiting ACOX1. Phytomedicine 2024;123:155183. doi:10.1016/j.phymed.2023.155183, PMID:37992491.
[16] Li XY, Xu MY, Chen Y, Liu S, Peng J, Wan Y, *et al*. Treatment of Metabolic Associated Fatty Liver Disease based on the Theory of "Liver Qi restricts the Whole Body Qi.". Clin J Tradit Chin Med 2023;35(4):709–713.
[17] Sun X, Chen XY. A case of non-alcoholic steatohepatitis complicated with liver fibrosis. Chin J Integr Tradit West Med Liver Dis 2022;32(3):277–278. doi:10.3969/j.issn.1005-0264.2022.03.025.
[18] Li S, Cai Q, Liu Q, Gong Y, Zhao D, Wan J, *et al*. Effective enhancement of the ability of Monascus pilosus to produce lipid-lowering compound Mona-

colin K via perturbation of metabolic flux and histone acetylation modification. Food Res Int 2024;195:114961. doi:10.1016/j.foodres.2024.114961, PMID:39277234.
[19] Li Y, Ouyang Q, Li X, Alolgal RN, Fan Y, Sun Y, *et al*. The Role of Gynostemma pentaphyllum in Regulating Hyperlipidemia. Am J Chin Med 2023;51(4):953–978. doi:10.1142/S0192415X23500441, PMID:37129524.
[20] Ding M, Zhou F, Li Y, Liu C, Gu Y, Wu J, *et al*. Cassiae Semen improves non-alcoholic fatty liver disease through autophagy-related pathway. Chin Herb Med 2023;15(3):421–429. doi:10.1016/j.chmed.2022.09.006, PMID:37538867.
[21] Qin S, Huang L, Gong J, Shen S, Huang J, Ren H, *et al*. Efficacy and safety of turmeric and curcumin in lowering blood lipid levels in patients with cardiovascular risk factors: a meta-analysis of randomized controlled trials. Nutr J 2017;16(1):68. doi:10.1186/s12937-017-0293-y, PMID:29020971.
[22] Zhao J, Jin J, Li Y, Zhang S, Li F, Cui J, *et al*. Yinchen-Gancao decoction ameliorated NASH in mice by reducing hepatic lipid accumulation, inhibiting hepatic inflammatory and endoplasmic reticulum stress. J Ethnopharmacol 2025;341:119318. doi:10.1016/j.jep.2025.119318, PMID:39755186.
[23] Liu XJ, Duan NN, Liu C, Niu C, Liu XP, Wu J. Characterization of a murine nonalcoholic steatohepatitis model induced by high fat high calorie diet plus fructose and glucose in drinking water. Lab Invest 2018;98(9):1184–1199. doi:10.1038/s41374-018-0074-z, PMID:29959418.
[24] Li X, Zhang H, Yu F, Xie S, Wang T, Zhang R, *et al*. IRF8 aggravates nonalcoholic fatty liver disease via BMAL1/PPARγ axis. Genes Dis 2025;12(3):101333. doi:10.1016/j.gendis.2024.101333, PMID:40083324.
[25] Zhang Y, Xie M, Wen J, Liang C, Song Q, Liu W, *et al*. Hepatic TM6SF2 activates antitumour immunity to suppress metabolic dysfunction-associated steatotic liver disease-related hepatocellular carcinoma and boosts immunotherapy. Gut 2025;74(4):639–651. doi:10.1136/gutjnl-2024-333154, PMID:39667906.
[26] Liang L, Rasmussen MH, Piening B, Shen X, Chen S, Röst H, *et al*. Metabolic Dynamics and Prediction of Gestational Age and Time to Delivery in Pregnant Women. Cell 2020;181(7):1680–1692.e15. doi:10.1016/j.cell.2020.05.002, PMID:32589958.
[27] Hakeem Said I, Truex JD, Heidorn C, Retta MB, Petrov DD, Haka S, *et al*. LC-MS/MS based molecular networking approach for the identification of cocoa phenolic metabolites in human urine. Food Res Int 2020;132:109119. doi:10.1016/j.foodres.2020.109119, PMID:32331646.
[28] Wang M, Carver JJ, Phelan VV, Sanchez LM, Garg N, Peng Y, *et al*. Sharing and community curation of mass spectrometry data with Global Natural Products Social Molecular Networking. Nat Biotechnol 2016;34(8):828–837. doi:10.1038/nbt.3597, PMID:27504778.
[29] Elapavalore A, Kondić T, Singh RR, Shoemaker BA, Thiessen PA, Zhang J, *et al*. Adding open spectral data to MassBank and PubChem using open source tools to support non-targeted exposomics of mixtures. Environ Sci Process Impacts 2023;25(11):1788–1801. doi:10.1039/d3em00181d, PMID:37431591.
[30] Wishart DS, Guo A, Oler E, Wang F, Anjum A, Peters H, *et al*. HMDB 5.0: the Human Metabolome Database for 2022. Nucleic Acids Res 2022;50(D1):D622–D631. doi:10.1093/nar/gkab1062, PMID:34986597.
[31] Sinclair E, Trivedi DK, Sarkar D, Walton-Doyle C, Milne J, Kunath T, *et al*. Metabolomics of sebum reveals lipid dysregulation in Parkinson's disease. Nat Commun 2021;12(1):1592. doi:10.1038/s41467-021-21669-4, PMID:33707447.
[32] Love MI, Huber W, Anders S. Moderated estimation of fold change and dispersion for RNA-seq data with DESeq2. Genome Biol 2014;15(12):550. doi:10.1186/s13059-014-0550-8, PMID:25516281.
[33] Yu G, Wang LG, Han Y, He QY. clusterProfiler: an R package for comparing biological themes among gene clusters. OMICS 2012;16(5):284–287. doi:10.1089/omi.2011.0118, PMID:22455463.
[34] Langfelder P, Horvath S. WGCNA: an R package for weighted correlation network analysis. BMC Bioinformatics 2008;9:559. doi:10.1186/1471-2105-9-559, PMID:19114008.
[35] Rebhan M, Chalifa-Caspi V, Prilusky J, Lancet D. GeneCards: integrating information about genes, proteins and diseases. Trends Genet 1997;13(4):163. doi:10.1016/s0168-9525(97)01103-7, PMID:9097728.
[36] Bauer-Mehren A, Rautschka M, Sanz F, Furlong LI. DisGeNET: a Cytoscape plugin to visualize, integrate, search and analyze gene-disease networks. Bioinformatics 2010;26(22):2924–2926. doi:10.1093/bioinformatics/btq538, PMID:20861032.
[37] Zhang Y, Zhou Y, Xu H, Jiang W, Li B, Lai D, *et al*. Therapeutic target database 2026: facilitating targeted therapies and precision medicine. Nucleic Acids Res 2026;54(D1):D1692–D1701. doi:10.1093/nar/gkaf1154, PMID:41243978.
[38] Gao K, Liu L, Lei S, Li Z, Huo P, Wang Z, *et al*. HERB 2.0: an updated database integrating clinical and experimental evidence for traditional Chinese medicine. Nucleic Acids Res 2025;53(D1):D1404–D1414. doi:10.1093/nar/gkae1037, PMID:39558177.
[39] Daina A, Michielin O, Zoete V. SwissADME: a free web tool to evaluate pharmacokinetics, drug-likeness and medicinal chemistry friendliness of small molecules. Sci Rep 2017;7:42717. doi:10.1038/srep42717, PMID:28256516.
[40] Daina A, Michielin O, Zoete V. SwissTargetPrediction: updated data and new features for efficient prediction of protein targets of small molecules. Nucleic Acids Res 2019;47(W1):W357–W364. doi:10.1093/nar/gkz382, PMID:31106366.
[41] Apweiler R, Bairoch A, Wu CH, Barker WC, Boeckmann B, Ferro S, *et al*. UniProt: the Universal Protein knowledgebase. Nucleic Acids Res 2004;32(Database issue):D115–D119. doi:10.1093/nar/gkh131, PMID:14681372.
[42] Szklarczyk D, Kirsch R, Koutrouli M, Nastou K, Mehryary F, Hachilif R, *et al*. The STRING database in 2023: protein-protein association networks and functional enrichment analyses for any sequenced genome of interest. Nucleic Acids Res 2023;51(D1):D638–D646. doi:10.1093/nar/gkac1000, PMID:36370105.
[43] Shannon P, Markiel A, Ozier O, Baliga NS, Wang JT, Ramage D, *et al*. Cytoscape: a software environment for integrated models of biomolecular interaction networks. Genome Res 2003;13(11):2498–2504. doi:10.1101/gr.1239303, PMID:14597658.
[44] Mullowney MW, Duncan KR, Elsayed SS, Garg N, van der Hooft JJJ, Martin NI, *et al*. Artificial intelligence for natural product drug discovery. Nat Rev Drug Discov 2023;22(11):895–916. doi:10.1038/s41573-023-00774-7, PMID:37697042.
[45] Berman HM, Westbrook J, Feng Z, Gilliland G, Bhat TN, Weissig H, *et al*. The Protein Data Bank. Nucleic Acids Res 2000;28(1):235–242. doi:10.1093/nar/28.1.235, PMID:10592235.
[46] Liu Y, Yang X, Gan J, Chen S, Xiao ZX, Cao Y. CB-Dock2: improved protein-ligand blind docking by integrating cavity detection, docking and homologous template fitting. Nucleic Acids Res 2022;50(W1):W159–W164. doi:10.1093/nar/gkac394, PMID:35609983.
[47] Pronk S, Páll S, Schulz R, Larsson P, Bjelkmar P, Apostolov R, *et al*. GROMACS 4.5: a high-throughput and highly parallel open source molecular simulation toolkit. Bioinformatics 2013;29(7):845–854. doi:10.1093/bioinformatics/btt055, PMID:23407358.
[48] Vogel K, Bläske T, Nagel MK, Globisch C, Maguire S, Mattes L, *et al*. Lipid-mediated activation of plasma membrane-localized deubiquitylating enzymes modulate endosomal trafficking. Nat Commun 2022;13(1):6897. doi:10.1038/s41467-022-34637-3, PMID:36371501.
[49] Zeng C, Liu J, Jin Z, Zhong S, Wu R, Luo H, *et al*. Spermidine suppresses liver fibrosis by remodeling the communication signal between liver sinusoidal endothelial cells and hepatic stellate cells. Cell Death Discov 2026;12(1):287. doi:10.1038/s41420-026-03129-4, PMID:42098063.
[50] Livak KJ, Schmittgen TD. Analysis of relative gene expression data using real-time quantitative PCR and the 2(-Delta Delta C(T)) Method. Methods 2001;25(4):402–408. doi:10.1006/meth.2001.1262, PMID:11846609.
[51] Kurien BT, Scofield RH. Western blotting. Methods 2006;38(4):283–293. doi:10.1016/j.ymeth.2005.11.007, PMID:16483794.
[52] Wu K, Liu Y, Xia J, Liu J, Wang K, Liang H, *et al*. Loss of SLC27A5 Activates Hepatic Stellate Cells and Promotes Liver Fibrosis via Unconjugated Cholic Acid. Adv Sci (Weinh) 2024;11(2):e2304408. doi:10.1002/advs.202304408, PMID:37957540.
[53] Kim HW, Wang M, Leber CA, Nothias LF, Reher R, Kang KB, *et al*. NPClassifier: A Deep Neural Network-Based Structural Classification Tool for Natural Products. J Nat Prod 2021;84(11):2795–2807. doi:10.1021/acs.jnatprod.1c00399, PMID:34662515.
[54] Hasenfuss SC, Bakiri L, Thomsen MK, Williams EG, Auwerx J, Wagner EF. Regulation of steatohepatitis and PPARγ signaling by distinct AP-1 dimers. Cell Metab 2014;19(1):84–95. doi:10.1016/j.cmet.2013.11.018, PMID:24411941.
[55] Wang J, Wang Z, Yu Y, Cheng S, Wu J. Advances in research on metabolic dysfunction-associated steatotic liver disease. Life Sci 2025;362:123362. doi:10.1016/j.lfs.2024.123362, PMID:39761743.
[56] Yang Z, Zhao J, Xie K, Tang C, Gan C, Gao J. MASLD development: From molecular pathogenesis toward therapeutic strategies. Chin Med J (Engl) 2025;138(15):1807–1824. doi:10.1097/CM9.0000000000003629, PMID:40640088.
[57] He Y, Chen Y, Qian S, van Der Merwe S, Dhar D, Brenner DA, *et al*. Immunopathogenic mechanisms and immunoregulatory therapies in MASLD. Cell Mol Immunol 2025;22(10):1159–1177. doi:10.1038/s41423-025-01307-5, PMID:40494889.
[58] Wang S, Cao M, Xu S, Shi J, Mao X, Yao X, *et al*. Luteolin Alters Macrophage Polarization to Inhibit Inflammation. Inflammation 2020;43(1):95–108. doi:10.1007/s10753-019-01099-7, PMID:31673976.
[59] Wang S, Cao M, Xu S, Shi J, Mao X, Yao X, *et al*. Luteolin Alters Macrophage Polarization to Inhibit Inflammation. Inflammation 2020;43(1):95–108. doi:10.1007/s10753-019-01099-7, PMID:31673976.
[60] Chen X, Han R, Hao P, Wang L, Liu M, Jin M, *et al*. Nepetin inhibits IL-1β induced inflammation via NF-κB and MAPKs signaling pathways in ARPE-19 cells. Biomed Pharmacother 2018;101:87–93. doi:10.1016/j.biopha.2018.02.054, PMID:29477475.
[61] Caporali S, De Stefano A, Calabrese C, Giovannelli A, Pieri M, Savini I, *et al*. Anti-Inflammatory and Active Biological Properties of the Plant-Derived Bioactive Compounds Luteolin and Luteolin 7-Glucoside. Nutrients 2022;14(6):1155. doi:10.3390/nu14061155, PMID:35334812.
[62] Lee D, Kwak HJ, Kim BH, Kim SH, Kim DW, Kang KS. Combined Anti-Adipogenic Effects of Hispidulin and p-Synephrine on 3T3-L1 Adipocytes. Biomolecules 2021;11(12):1764. doi:10.3390/biom11121764, PMID:34944408.
[63] Zhong J, Ji X, Zhao Y, Jia Y, Song C, Lv J, *et al*. Identification of BAF60b as a Chromatin-Remodeling Checkpoint of Diet-Induced Fatty Liver Disease. Diabetes 2024;73(10):1615–1630. doi:10.2337/db24-0002, PMID:39046829.
[64] Tanaka T, Masuzaki H, Ebihara K, Ogawa Y, Yasue S, Yukioka H, *et al*. Transgenic expression of mutant peroxisome proliferator-activated receptor gamma in liver precipitates fasting-induced steatosis but protects against high-fat diet-induced steatosis in mice. Metabolism 2005;54(11):1490–1498. doi:10.1016/j.metabol.2005.05.015, PMID:16253638.
[65] Liu J, Cinar R, Xiong K, Godlewski G, Jourdan T, Lin Y, *et al*. Monounsaturated fatty acids generated via stearoyl CoA desaturase-1 are endogenous inhibitors of fatty acid amide hydrolase. Proc Natl Acad Sci U S A 2013;110(47):18832–18837. doi:10.1073/pnas.1309469110, PMID:24191036.
[66] Liu Y, Wang S, Younas A, Lv J, Al Mamun A, Shao C. The effects and mechanisms of Xiaoyao San on nonalcoholic fatty liver disease rat based

on transcriptomics and proteomics analysis. Sci Rep 2025;15(1):10478. doi:10.1038/s41598-025-91890-4, PMID:40140444.
[67] Cai FF, Wu R, Song YN, Xiong AZ, Chen XL, Yang MD, *et al*. Yinchenhao Decoction Alleviates Liver Fibrosis by Regulating Bile Acid Metabolism and TGF-β/Smad/ERK Signalling Pathway. Sci Rep 2018;8(1):15367. doi:10.1038/s41598-018-33669-4, PMID:30337590.
[68] Schattenberg JM, Bedossa P, Guy CD, Taub R, Labriola D, Zhang H, *et al*. Quantitative regression of qFibrosis with resmetirom: Exploratory histologic endpoints from the MAESTRO-NASH phase III clinical trial. J Hepatol 2026;85(2):202–211. doi:10.1016/j.jhep.2026.03.021, PMID:41895606.
[69] Harrison SA, Bedossa P, Guy CD, Schattenberg JM, Loomba R, Taub R, *et al*, MAESTRO-NASH Investigators. A Phase 3, Randomized, Controlled Trial of Resmetirom in NASH with Liver Fibrosis. N Engl J Med 2024;390(6):497–509. doi:10.1056/NEJMoa2309000, PMID:38324483.
[70] Fiorucci S, Urbani G, Distrutti E, Biagioli M. Obeticholic Acid and Other Farnesoid-X-Receptor (FXR) Agonists in the Treatment of Liver Disorders. Pharmaceuticals (Basel) 2025;18(9):1424. doi:10.3390/ph18091424, PMID:41011291.
[71] Wang K, Zhang Y, Wang G, Hao H, Wang H. FXR agonists for MASH therapy: Lessons and perspectives from obeticholic acid. Med Res Rev 2024;44(2):568–586. doi:10.1002/med.21991, PMID:37899676.
[72] Xu FP, Yang C, Yu SH, Cai H, Hui MY, Fang LL, *et al*. Yinchenhao Decoction, a compound Chinese herbal medicine, for patients with nonalcoholic fatty liver disease: A randomized, double-blind, placebo-controlled trial. J Integr Med 2026;24(3):365–375. doi:10.1016/j.joim.2026.03.003, PMID:41905832.
[73] Lei L, Wang B, Zhao L, Li J, Yan X, Jiang J, *et al*, BRAVO Collaborative Group. Berberine and Adiposity in Diabetes-Free Individuals With Obesity and MASLD: A Randomized Clinical Trial. JAMA Netw Open 2026;9(1):e2554152. doi:10.1001/jamanetworkopen.2025.54152, PMID:41543854.